Experimental constraints on the outgassing dynamics of basaltic magmas

Pioli, Laura; Bonadonna, Costanza; Azzopardi, B. J.; Phillips, J. C.; Ripepe, M.

How to cite

PIOLI, Laura et al. Experimental constraints on the outgassing dynamics of basaltic magmas. In: Journal of geophysical research, 2012, vol. 117, n° B3. doi: 10.1029/2011JB008392

This publication URL: https://archive-ouverte.unige.ch/unige:19462
Publication DOI: 10.1029/2011JB008392

Experimental constraints on the outgassing dynamics of basaltic magmas

L. Pioli,[1] C. Bonadonna,[1] B. J. Azzopardi,[2] J. C. Phillips,[3] and M. Ripepe[4]

Received 28 March 2011; revised 29 December 2011; accepted 9 January 2012; published 8 March 2012.

[1] The dynamics of separated two-phase flow of basaltic magmas in cylindrical conduits has been explored combining large-scale experiments and theoretical studies. Experiments consisted of the continuous injection of air into water or glucose syrup in a 0.24 m diameter, 6.5 m long bubble column. The model calculates vesicularity and pressure gradient for a range of gas superficial velocities (volume flow rates/pipe area, 10^{-2}–10^{2} m/s), conduit diameters (10^{0-2} m), and magma viscosities (3–300 Pa s). The model is calibrated with the experimental results to extrapolate key flow parameters such as C_o (distribution parameter) and Froude number, which control the maximum vesicularity of the magma in the column, and the gas rise speed of gas slugs. It predicts that magma vesicularity increases with increasing gas volume flow rate and decreases with increasing conduit diameter, until a threshold value (45 vol.%), which characterizes churn and annular flow regimes. Transition to annular flow regimes is expected to occur at minimum gas volume flow rates of 10^{3}–10^{4} m^3/s. The vertical pressure gradient decreases with increasing gas flow rates and is controlled by magma vesicularity (in bubbly flows) or the length and spacing of gas slugs. This study also shows that until conditions for separated flow are met, increases in magma viscosity favor stability of slug flow over bubbly flow but suggests coexistence between gas slugs and small bubbles, which contribute to a small fraction of the total gas outflux. Gas flow promotes effective convection of the liquid, favoring magma homogeneity and stable conditions.

Citation: Pioli, L., C. Bonadonna, B. J. Azzopardi, J. C. Phillips, and M. Ripepe (2012), Experimental constraints on the outgassing dynamics of basaltic magmas, *J. Geophys. Res.*, *117*, B03204, doi:10.1029/2011JB008392.

1. Introduction

[2] Basaltic eruptive activity is highly variable in intensity, ranging from low-energy lava effusion, fire fountaining, and intermittent Strombolian explosions, to more energetic ash-forming violent Strombolian, subplinian, and Plinian activity. Moreover, unlike silica-rich volcanism, there is no direct relationship between explosivity and magma flux, due to the complex interplay between gas segregation, initial gas content of the magma, and ascent rate. The low viscosity of basaltic magmas allows for separated two-phase (liquid and gas) flows, which play a fundamental role in the shallow conduit and explosive dynamics. In particular, bubble concentration (and its vertical and lateral gradients), bubble size distribution, and vertical pressure drop within the magma column at shallow levels control the gas rise dynamics and, consequently, define the eruptive style and explosivity. For example, intermittent explosions may be generated when the pattern is periodic (i.e., characterized by regular temporal and spatial fluctuations), and the pressure drop within the magma column and the rise rate (which controls degassing) also control overpressure buildup, together with near surface region processes [*James et al.*, 2008].

[3] Previous studies have described the main categories of basaltic explosive eruptions (i.e., Hawaiian and Strombolian) in terms of different two-phase flow regimes in the volcanic conduit (bubbly, intermittent, and annular flow) [*Vergniolle and Jaupart*, 1986; *Jaupart and Vergniolle*, 1989; *Parfitt and Wilson*, 1995; *Vergniolle and Mangan*, 2000, Figure 1]. Each pattern is defined by a peculiar geometry of the distribution and dynamics of gas and liquid phases, which will be described in details in section 1.1. In particular, slug flow is expected for Strombolian eruptions; Hawaiian eruptions have been explained in terms of homogeneous two-phase flows (where the gas segregation is suppressed by high magma ascent velocity [*Wilson and Head*, 1981]) or annular flows [*Vergniolle and Jaupart*, 1986]. These studies were also confirmed by evidences from real eruptions [*Blackburn et al.*, 1976; *Mangan and Cashman*, 1996; *Vergniolle and Brandeis*, 1996; *Polacci et al.*, 2006]. Transition between conduit flow patterns is

[1]Section des Sciences de la Terre et de l'Environnement, Université de Genève, Geneva, Switzerland.
[2]Process and Environmental Engineering Research Division, Faculty of Engineering, University of Nottingham, Nottingham, UK.
[3]Department of Earth Sciences, University of Bristol, Bristol, UK.
[4]Dipartimento di Scienze della Terra, Università di Firenze, Florence, Italy.

0148-0227/12/2011JB008392

also believed to determine sudden changes of eruptive style, switch from pulsatory to continuous activity, and variations in explosivity [*Vergniolle and Mangan*, 2000; *Parfitt*, 2004; *Polacci et al.*, 2006; *Parfitt and Wilson*, 1995; *James et al.*, 2009; *Lyons et al.*, 2010].

[4] The stability and characteristics of two-phase flow patterns in low-viscosity magmatic flow is typically predicted based on fluid dynamical models developed from a combination of theoretical studies and experiments using very low viscosity (10^{-5}–10^{0} Pa s) and low surface tension ($\sim 10^{-2}$ N/m) liquids flowing along small diameters (a few centimeters) pipes [*Seyfried and Freundt*, 2000; *Jaupart and Vergniolle*, 1989; *James et al.*, 2004, 2009]. These experiments, however, due to incomplete scaling to magmatic systems, were appropriate only for the investigation of specific aspects of the flow dynamics.

[5] More general theoretical models on separated two-phase flow dynamics along vertical pipes have been implemented for engineering applications. They are based on models appropriate for inertially dominated flows and include turbulence effects, which influence coalescence and breakup rates and control the maximum size of stable bubbles [*Brown*, 1965; *Wallis*, 1969; *Taitel et al.*, 1980; *Mishima and Ishii*, 1984; *McQuillan and Whalley*, 1985; *Spedding et al.*, 1998].

[6] Other models also account for gas segregation mechanisms occurring in the upper portion of the magma chamber, leading to the formation of foam layers [*Jaupart and Vergniolle*, 1989], or at sills and dykes [*Menand and Phillips*, 2007; *Pioli et al.*, 2009]. Gas segregation is mostly efficient at very low magma eruption rates, where the bubble slip velocity (i.e., the velocity of the bubble relative to the liquid) approaches or equals the average bubble velocity, favoring outgassing processes. In these conditions, separated two-phase flow dynamics is expected to control the volcanic activity, and, for constant magma and gas supply rates, eruptive style will be controlled by shallow conduit processes.

[7] These conditions are expected at several basaltic volcanoes, which are typically characterized by constant passive degassing from the central vent during interruptive times (Masaya, Miyakejima, Stromboli, Kilauea, Etna) [*Allard et al.*, 1991, 1994; *Burton et al.*, 2000; *Kazahaya et al.*, 2004; *Stevenson and Blake*, 1998]. Open-conduit degassing from a single volcano is responsible of emission of 10^{0} to 10^{3} tons of gas per day, consisting in a mixture of H_2O, CO_2 S, Cl, and F rich gases [*Aiuppa et al.*, 2006; *Gerlach et al.*, 2002] and can represent a significant contribution on the global volcanic emission (for example, up to 8% by mass in the case of Etna volcano [*Allard et al.*, 2002]).

[8] Recent improvements of thermal, video, radar, and acoustic monitoring techniques have provided new powerful tools for the study of outgassing processes and made available geophysical and geochemical data sets for many central volcanoes, such as Stromboli and Etna (Italy), Kilauea (Hawaii), and Villarrica (Chile). These studies reveal that outgassing is an unsteady, often pulsatory process, characterized by fluctuations in both intensity and composition of the emitted gases [*Harris and Ripepe*, 2007; *Ripepe et al.*, 2010, 2002; *Edmonds and Gerlach*, 2007]. However, unambiguous interpretation of infrasound and gas flux measurements in terms surface activity in terms of subsurface flow dynamics responsible is not yet possible due to the limited knowledge of the parameter values that control changes in the separated flow processes in magmas. As a result, it is still not possible to infer the conduit flow regimes and properties from volcano monitoring data and to predict the effect of abrupt shifts in gas and magma flow rates at open conduit volcanoes or during eruptive events in terms of conduit flow and eruption dynamics.

[9] To address this issue, we performed a series of large-scale laboratory experiments and develop a general model for gas rise dynamics into basaltic magmas in cylindrical conduits to gain further insights into (1) how coalescence and segregation of gas bubbles control the flow dynamics, (2) the expected vesicularity and conduit flow pattern characteristics and stability for a range of gas flow rates, and (3) the effect of these processes on volcanic degassing dynamics. These experiments were done within stagnant liquid (i.e., bubbly column dynamics) to ensure ideal conditions for separated flow and are ideally scaled to outgassing dynamics, but the flow general properties can be extrapolated also to regimes with liquid outflux [*Mudde and Saito*, 2001] and might potentially be applied to describe eruptive regimes characterized by separated two-phase flow dynamics.

[10] This is the first study coupling large-scale experiments and high viscosity (300 Pa s) liquids. These experiments allowed for accurate scaling to magmatic conditions (as explained in section 2.2); the calibration of fundamental parameters and constants and testing of the applicability of more general models [*Zuber and Findlay*, 1965; *Wallis*, 1969] to the two-phase flow dynamics of basaltic magmas in volcanic conduits (described in sections 4 and 5). In the next section, we summarize two-phase flow regimes in vertical pipe flow from engineering studies, before describing the experimental method in section 2. In section 3 we present the experimental results, and we present their analysis in section 4. In section 5 we describe the application to volcanic systems, before highlighting the main conclusions in section 6.

1.1. Two-Phase Flow Regimes in Vertical Conduits for Low-Viscosity Magmas

[11] When magma containing exsolved volatiles rises through the upper conduit, different flow regimes or patterns develop. Each pattern is defined by a peculiar geometry of the distribution and dynamics of gas and liquid phases. In silicic magmas, expected flow regimes are homogenous bubbly flow (characterized by noninteracting bubbles distributed in the liquid) and dispersed flow (i.e., liquid drops dispersed in the gas phase), separated by the fragmentation level [*Sparks*, 1978]. Permeable flow can also occur through interconnected gas bubbles [*Jaupart and Allègre*, 1991; *Saar and Manga*, 1999; *Blower*, 2001; *Rust and Cashman*, 2004; *Melnik et al.*, 2005], favoring outgassing and effusive eruptions. Individual gas bubbles can separate from the liquid in low-viscosity magmas (e.g., mafic and carbonatitic) and generate a more complex series of flow patterns, which can be grouped into bubbly, intermittent, and annular flows [*Vergniolle and Mangan*, 2000]. These flow patterns have been originally described for water-air flows [*Hewitt and Hall-Taylor*, 1970, Figure 1].

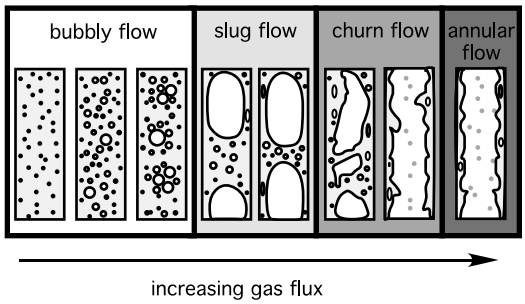

Figure 1. Idealized vertical two-phase flow patterns for basaltic magmas in vertical conduits. Liquid is shown in gray and gas bubbles are shown in white. For low gas flow rates, the bubbles do not interact and have uniform distribution; with increasing flow rates their concentration increases and coalescence becomes efficient creating a population of bubbles with different sizes. In slug flow, gas slugs have symmetrical shapes and smooth wake [*Viana et al.*, 2003]. With increasing gas flow rate, the slugs get closer until the gas can locally drag the liquid at the walls of the slugs, and the flow becomes unstable. At annular flow conditions, the liquid is dragged upward by the gas, which forms an internal annulus.

[12] The main factors controlling the two-phase flow patterns are the liquid and gas fluxes, conduit geometry, liquid properties, bubble coalescence, liquid and gas entrainment, but also the entrance conditions at the bottom of the pipe [*Lucas et al.*, 2005; *Delnoij et al.*, 1997; *Kozma*, 1995; *Vijayan et al.*, 2001]. Regular oscillations of flow properties (given by variations of gas volumetric fraction and instabilities at liquid/gas interfaces) are characteristics of all patterns and control the pattern transition mechanisms [*James et al.*, 2004]. The transition between flow patterns can be described not only in terms of volume or mass fluxes of the phases but also pressure drop, vertical and lateral variation of void fraction, and periodicities in the flow [*Song et al.*, 1995; *Costigan and Whalley*, 1997; *Ohnuki and Akimoto*, 2000; *Omebere-Iyari et al.*, 2007]. At the lowest gas flux the flow is bubbly, with small, noninteracting bubbles rising through the fluid; coalescence occurs with increasing gas volume fraction and bubble clusters can form "waves" of bubble-rich and bubble-poor liquid [*Manga*, 1996]. With further increase of the gas volume flux, bubbles in areas of high concentration can coalesce into single, conduit-filling, bubbles that characterize slug flows, which are called Taylor bubbles or gas slugs (Figure 1). In slug flows, liquid moves downward along the conduit walls to allow upward movement of the gas slug. Individual gas slugs are separated by liquid that contain dispersed bubbles whose length increases and spacing decreases with increasing gas flux [*Fabre and Liné*, 1992; *Paglianti et al.*, 1996]. The flow becomes unstable when the gas fraction is sufficient to allow local liquid "flooding" (i.e., the liquid is carried upward by the gas) [*Wallis*, 1969; *McQuillan and Whalley*, 1985; *Guedes de Carvalho and Ferreira*, 2000]. Flows characterized by the simultaneous downward and upward motion of the liquid film at different points along the pipe walls are highly unstable and called churn flow. Further increases in gas flux promote annular flow, characterized by a central gas phase and upward movement of all the liquid film along the pipe walls because the gas phase has enough energy to fully support the liquid [*Hewitt and Hall-Taylor*, 1970; *Barbosa et al.*, 2001]. Liquid droplets are incorporated into the central gas flux by shearing at the liquid-gas interface. The competition between droplet entrainment and deposition determines the liquid film thickness along the walls [*Azzopardi and Wren*, 2004]. It is important to notice that changes in gas composition should not relevantly affect the stability and characteristic of flow patterns, as most of the properties depend on the density difference between the magma and gas phase.

1.2. Regime Transitions

[13] In separated two-phase flows, transitions between flow regimes are due to bubble migration and coalescence. For any given set of conditions, the bubble size distribution depends on bubble nucleation and growth by diffusion and expansion and the balance between bubble coalescence and breakup [*Grevskott et al.*, 1996; *Lehr et al.*, 2002]. Bubble coalescence rate Γ is the sum of the contributions related to turbulence, buoyancy, and laminar flow effects, and for a population of bubbles of class sizes i, j it can be computed as [*Prince and Blanch*, 1990]:

$$\Gamma = \frac{1}{2}\sum_i \sum_j \left\{ \left(\theta_{ij}^T + \theta_{ij}^B + \theta_{ij}^L \right) \times \exp\left(-t_{ij}/T_{ij}\right) \right\} \qquad (1)$$

where θ^T, θ^B, θ^L are the collision frequencies between bubbles related to turbulence, buoyancy, and laminar flow, respectively, t is the coalescence time, and T is the bubble contact time. Bubbles interact with each other due to velocity fluctuations (turbulence effects), differential rise velocity due to size differences (buoyancy effects), and lateral velocity gradients (laminar shear effects). In very general terms, the lower the viscosity of the fluid, the higher the collision rate, but the lower the contact time and hence coalescence rate. Bubble breakup rate depends on the combination of turbulence, shearing, and surface instability [*Clift et al.*, 1978; *Stein and Spera*, 1992].

[14] Bubble breakup determines the maximum stable bubble diameter ($d_{b,\max}$) and is also important for stability of slug flow when the pipe diameter $D \geq d_{b,\max}$ (which was the case for our water-airflow experiments). When $D \geq d_{b,\max}$ the expected flow patterns, with increasing volume gas fluxes, are bubbly to churn to annular and dispersed [*Ohnuki and Akimoto*, 2000; *Omebere-Iyari et al.*, 2007].

[15] In high Reynolds number flows, bubble breakup is mainly related to turbulence processes, resulting in a maximum stable bubble size which depends on the size (and energy) of the turbulent eddies; the eddies can transport small bubbles, but break bubbles with diameters similar or slightly larger than their size, and do not affect larger bubbles [*Hinze*, 1955; *Prince and Blanch*, 1990; *Hesketh et al.*, 1991; *Colella et al.*, 1999]. Owing to the large experimental data set available for these types of flows from engineering studies, several numerical models have been developed for the quantification of this process [*Colella et al.*, 1999; *Olmos et al.*, 2001; *van den Hengel et al.*, 2005]. Shear related breakup requires high instantaneous velocity gradients and therefore is expected to be mostly relevant for small bubbles confined in the liquid

film in annular and churn flow or at the sides of the gas slug in slug flow, and it likely plays a minor role in flow pattern stability. In low Reynolds numbers, separated two-phase flows, formation of Rayleigh-Taylor instabilities on the bubble-liquid interface is the main mechanism controlling maximum bubble size [*Clift and Grace*, 1972; *Clift et al.*, 1978]. These instabilities, in fact, form perturbations at the interface which grow deeper eventually leading to bubble splitting. In general, the maximum stable bubble size increases with increasing liquid viscosity and surface tension, which decreases Reynolds numbers and the wavelength of interface instabilities.

[16] Unfortunately, existing models that describe the required conditions for bubble rupture do not take into account bubble interaction and wall effects and consequently might underestimate the maximum diameter. For example, *Clift et al.* [1978] suggest a maximum stable diameter of 4.9 cm for air bubbles in water but stable slug flow has been observed in vertical pipes with a diameter of 7.2 cm, and in a 20 cm diameter pipe, where the ratio between the pipe length and diameter L/D exceeded 100 [*Guet et al.*, 2002; *Shen et al.*, 2010]. The rise of a single gas slug was also observed in a 25 cm diameter pipe [*James et al.*, 2011]. Therefore it is not clear what the effect of pipe walls on the stability of large bubbles may be and what is the minimum pipe length required to reproduce stable slug flow under experimental conditions. More experimental work is needed to infer the maximum pipe diameter that allows for slug flow stability for very viscous fluids and magmas in vertical conduits. On the other hand, the minimum bubble diameters in the distributions depend not only on the breakup mechanisms (i.e., the size of the newly formed bubbles), and, in the case of noninteracting bubbles in dilute suspensions, to gas expansion effects but in the case of magmas, also to bubble nucleation dynamics.

[17] Transitions between two-phase flow regimes were first quantified in terms of gas and liquid mass flux [*Hewitt and Roberts*, 1969] and then in terms of superficial liquid and gas velocities, which are the components of the velocity of the mixture V_m:

$$V_m = u_{sl} + u_{sg} \tag{2}$$

where u_{sl} and u_{sg} are the superficial gas and liquid velocities and are defined as:

$$u_s = \frac{Q}{A} \tag{3}$$

where u_s is the superficial velocity, Q is the volume flux, and A is the pipe cross-sectional area. The real velocities of the phases are

$$u_g = \frac{u_{sg}}{\varepsilon_g} \tag{4}$$

$$u_l = \frac{u_{sl}}{1 - \varepsilon_g} \tag{5}$$

where $u_{l,g}$ are the real velocities of the gas and liquid and ε_g is the average gas volume fraction. Superficial velocities have been used directly to model bubble concentration and flow dynamics [*Taitel et al.*, 1980; *Mishima and Ishii*, 1984].

2. The Experimental Apparatus and Flow Parameters

[18] Experiments were conducted on a 6.5 m high cylindrical transparent acrylic resin bubble column with cross section diameter of 0.24 m (Figure 2). The gas inlet system consisted of 25, individually controlled, 5 mm diameter nozzles with circular cross section. The nozzles were positioned in three rings with 4, 8, and 12 nozzles each. The 25th was at the center of the column. The diameters of the rings were selected so that each nozzle was in the middle of 1/25th of the column cross-sectional area. Gas flow was measured using up to five rotameters to ensure equal distribution of gas at the bottom of the column during experiments using multiple nozzles. Absolute pressure was monitored using four, equally spaced, Keller PD-25 sealed gauge pressure transmitters installed along the column (Figure 2). The temperature of the mixture was also monitored at 1.5 and 2.9 m from the base to ensure that there were no thermal gradients since the viscosity of the liquids used changes with temperature. Average gas volume fraction of the column at stable flow conditions was calculated by comparing initial liquid height at zero gas flux and the final height (when the column height was oscillating, both minimum, maximum, and average height were measured) with the aid of a vertical scale which was attached to the column external wall.

[19] Experiments consisted of generating a range of fluxes of air through stagnant liquid which was either water, glucose syrup (Cargill "C star sweet"), or a mixture of the two. Gas volume flux ranged from $\sim 10^{-4}$ to 10^{-1} m^3/s, corresponding to superficial gas velocities from $\sim 10^{-2}$ to 1.9 m/s for water experiments and $\sim 10^{-2}$ to 0.7 m/s for syrup experiments. The main physical characteristics of the liquids are summarized in Table 1. Pure glucose syrup viscosity has a shear thinning rheology, which was measured with a rotational viscometer. The shear rate in bubble columns is a linear function of superficial gas velocity [*Nishikawa*, 1991] and, because of the limited range of gas flow rates in the experimental conditions, the syrup viscosity can be approximated to a constant value of 300 Pa s. The rheology of the mixtures of water and glucose syrup was Newtonian, and their bubble-free viscosity was measured after each experiment.

2.1. Initial Bubble Size and Entrance Effects

[20] The initial dimension of a bubble generated from an orifice in a stagnant liquid depends on the gas volumetric flow rate and the physical properties of both liquid and gas phases. It can be calculated by balancing the bubble growth rate and the rise speed [*Davidson and Schüler*, 1960]. When compared with nozzle spacing for different configurations (with 25, 20, 10, or 5 active, equally spaced nozzles), the calculations for initial bubble diameters show that for $u_{sg} \geq$ 0.1 m/s, and when all the nozzles are active, bubbles in syrup interact with each other in the inlet area and coalesce at the base of the column, forming a single large bubble. For lower u_{sg}, the bubbles generated are smaller than the spacing between nozzles. This phenomenon could slightly favor the stability of slug flow in the experimental conditions.

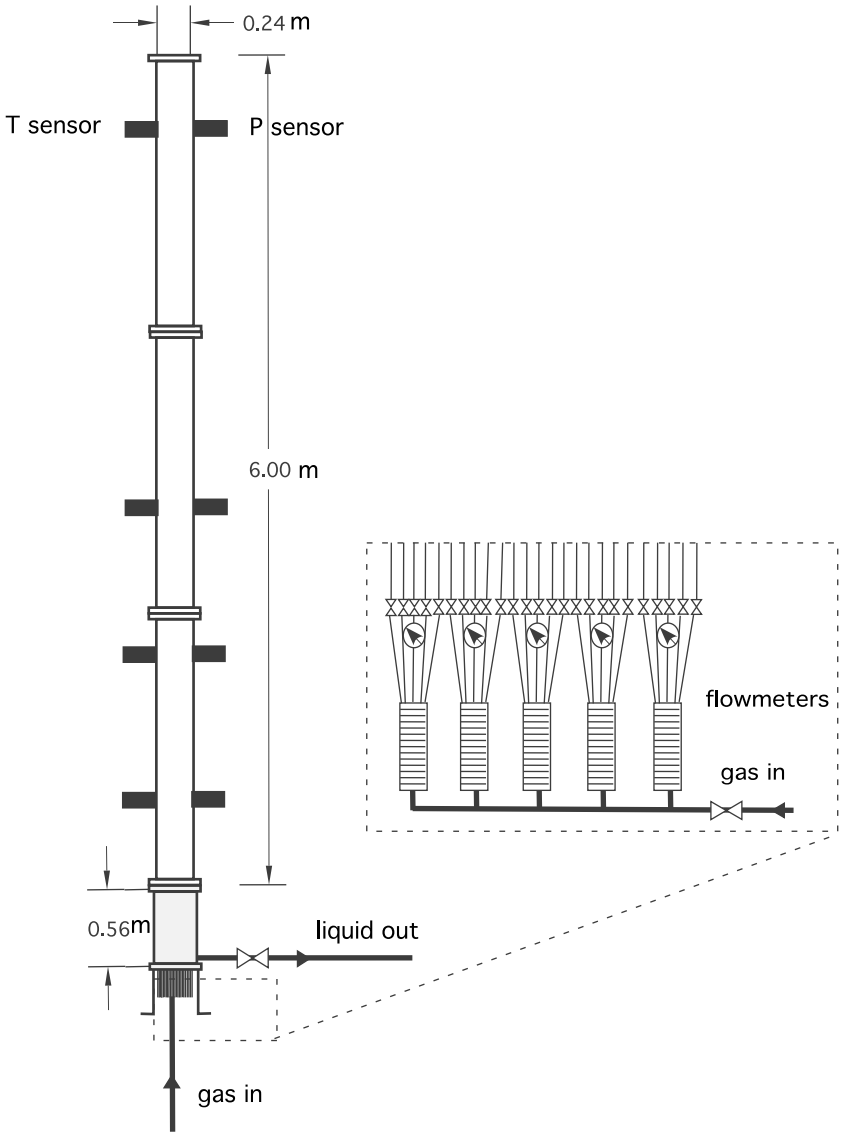

Figure 2. Experimental apparatus.

2.2. Applicability and Limitations of the Experiments to Magmatic Conditions

[21] The applicability of our experiments to describe outgassing of basaltic magma can be discussed in terms of geometric and dynamic similarity. Geometric similarity requires that flow scale (as quantified by pipe height/diameter ratio, bubble diameter/pipe diameter ratio) is large enough to be able to reproduce flow phenomena within the upper portion of the volcanic edifice. Dynamic scaling requires that the flow regime, as defined by the relative effects of the forces acting on the flow, matches the expected conditions for the natural system. In addition, the bubble size range (which depends on both initial bubble diameter and bubble interaction processes) controls bubble rise speed and pressure drop in the column (which depend on the column height and mixture density).

Table 1. Physical Characteristics of the Liquids Used Compared With Average Features Basaltic Magmas[a]

Liquid	Density (Kg/m^3)	Rheology	Viscosity (Pa s)	Surface Tension (N/m)
Water$^+$	1000	Newtonian	8.9×10^{-4}	7×10^{-2}
Glucose syrup	1450	Shear thinning	3.0×10^{2}	8×10^{-2}
Basaltic magma	~2800	Variable!	10^{0}–10^{2}	4×10^{-1}
Mixture 1	1350	Newtonian	6.5	8×10^{-2}
Mixture 2	1420	Shear thinning	2×10^{2}	8×10^{-2}
Mixture 3	1410	Shear thinning	2.8×10^{2}	8×10^{-2}

[a]For syrup, the value of viscosity refers to experimental conditions.

Table 2. Expected Values of Eotvos, Morton, Froude, Bubble Reynolds Numbers, and Nondimensional Viscosity for Our Experiments and During Basaltic Eruptions[a]

	Eo	*Mo*	*Fr*	N_η	Re_{max}
Basaltic eruptions	10^0–10^4	10^5–10^{10}	0.1–0.351	10^1–10^3	10–10^4
Experiments- water/air	10^2–10^3	2.5×10^{-11}	0.351	2×10^{-2}	10^3–10^6
Experiments-syrup/air	10^{-1}–10^5	2.2×10^{10}	0.23	4×10^2	10^0
Experiments mixture/air	10^{-1}–10^4	10^5–10^{10}	0.23–0.351	10^1–10^2	10^0–10

[a]Eotvos is *Eo*, Morton is *Mo*, Froude is *Fr*, Bubble Reynolds numbers are *Re*, and nondimensional viscosity is N_η. Regimes from basaltic eruptions are taken from *Seyfried and Freundt* [2000]. Minimum *Eo* is calculated for millimeter-size bubbles. *Fr* number for basaltic magma as derived by *Seyfried and Freundt* [2000].

[22] Regime transitions and stability of slug flow are also strong function on the experimental pipe length/diameter ratio (L/D); in fact, gas slugs are expected to form for any flow conditions in an infinite length pipe because bubbles will have an infinite time to interact and will eventually coalesce into slugs [*Wallis*, 1969]. However, stable conditions for regime transitions have been reached for water airflows in experiments with L/D between 8 and 29.9 and greater [*Lucas et al.*, 2005]. For the liquids used here with viscosities significantly higher than water, the minimum L/D required for flow stability has not been investigated, but it is expected to be lower, due to increased coalescence efficiency. In our experiments, the maximum L/D ranged from 9 to 25; within this interval, no variation of the stability of the flow patterns was observed in glucose syrup experiments, suggesting that they can be considered to be representative for longer pipes. Moreover, it is also important to consider that cylindrical volcanic conduit geometry is likely only for the shallow part of volcanic edifices [*Keating and Valentine*, 2008; *Ryan*, 1988]. For these reasons, the experiments can investigate the dynamics of gas rise only along the last few hundreds meters of the conduit. Also, the total pressure drop in our experiments is limited, and near surface gas expansion effects are not fully reproduced.

[23] Relevant dimensionless parameters for the flow dynamics are bubble Eotvos number (*Eo*), which is the ratio between buoyancy and surface tension forces; Morton number (*Mo*), relating viscous to surface tension forces; Froude (*Fr*), which is the ratio of inertia and gravitational forces; and Reynolds number (*Re*) which is the ratio of inertial to viscous forces and dimensionless inverse viscosity (N_η) [*Wallis*, 1969; *Clift et al.*, 1978] (expected values are shown in Table 2). Glucose syrup-air experiments satisfactorily reproduce natural conditions expected for magmatic flow during outgassing or mild Strombolian explosions of basaltic magma, whereas water-air experiments are dominated by inertia and have limited similarity with the natural system. The initial bubble size and, in particular, the bubble dimensionless diameter, which is the ratio between bubble and pipe diameters D_b/D, is considered as another critical parameter for bubble coalescence and flow regime stability [*Cheng et al.*, 2002; *Liu*, 1993]. Bubble rise speed is, in fact, a function of the rheological properties of the two phases but is also directly proportional to the squared diameter of the bubble itself (when $Eo < 0.2$) or to its square root for higher Eotvos number [*Clift et al.*, 1978]. Textural studies on basaltic scoria ejected by mild Strombolian explosions have measured a vesicle range of tens of millimeters to a few centimeters [*Andronico et al.*, 2008; *Lautze and Houghton*, 2005], corresponding to minimum bubble dimensionless diameters of 10^{-1}–10^4, but larger bubbles have been observed bursting at the magma surface [*Vergniolle and Brandeis*, 1996]. In our experiments the initial bubble diameters ranged from centimeters to millimeters size with corresponding dimensionless bubble size ranges of 10^0–10^{-3}, which ensure a good reproduction of expected surface conditions for passive degassing.

[24] The rheological effects related to magma cooling and crystallization and bubble growth by diffusion processes were not investigated in our experiments and thus conditions for thermodynamic similarity were not considered.

3. Results

3.1. Two-Phase Flow Patterns

[25] Two-phase flow patterns in our water-air and glucose-air experiments were primarily identified through direct observations and analyzed in terms of average gas volume fraction and pressure gradient measurement. The experiments showed a clear dependence on the stability of two-phase flow patterns on liquid viscosity, both in terms of transition conditions and observed patterns.

[26] In water airflows, bubbly flow was observed for low u_{sg}, and transition to churn flow was observed at u_{sg} $\sim$1.4 m/s. The absence of slug flow is related to instability of large bubbles due to inertial effects and is in accordance with experimental observations of direct transition from bubbly to churn flow in vertical pipes with diameters larger than 10 cm and similar L/D [*Cheng et al.*, 1998; *Ohnuki and Akimoto*, 2000; *Omebere-Iyari et al.*, 2007]. In all experiments, liquid circulation within the column was marked by turbulent structures developing at the conduit peripheries, clearly visible at the walls. The structures developed throughout the whole column height; the size of eddies (from a few to >20 cm) decreased with increasing gas flux. Churn flow conditions were marked by strong turbulence and up to 30 cm column height fluctuations, whereas in bubbly flow, column height oscillations were limited to a few centimeters. A mist formed by a liquid spray was produced at the top of the liquid column.

[27] In pure syrup and syrup mixtures-airflows, large bubbles formed at the base of the column when superficial gas velocities exceeded 5×10^{-3} m/s. True slug flow conditions (i.e., formation of gas slugs) were attained for $u_{sg} \geq 10^{-2}$ m/s. With increasing gas flow rate, the length of the slugs increased and the spacing between two consecutive slugs decreased. Liquid at the pipe walls was driven downward by the rise of the slugs and decimeter- to meter-sized circulation cells developed leading to efficient recirculation along the whole column height. Transition to churn flow was

Figure 3. Sheared bubbles visible at the pipe walls during a syrup-air experiment (u_{sg} = 0.06 m/s). Scale bar is 2 cm long.

observed at u_{sg}~0.4 m/s for pure syrup and >0.9 m/s for the lowest viscosity mixture 1 (Table 1). The transition was marked by the onset of instability of the liquid film surrounding the gas slugs, which was reduced to a few centimeters. The film was locally dragged upwards by the gas flux and more complex dynamics of the liquid circulation pattern developed, leading to discontinuous shearing and variable lengths of the gas slugs, which had heights between 2 m to several meters (for high gas volume rates they could also be as long as the column). Small quantities of fine mist were observed forming at the top of the column at the highest gas fluxes. The distance between two different slugs was always <10 cm. Very small (submillimeter to centimeter size) bubbles coexisted with the gas slugs in all of our experiments with glucose syrup. Most were too small to move independently from the liquid and were transported in the liquid circulation pattern and sheared at the pipe walls (Figure 3). To ensure that small bubbles were not inherited from trapping of air during pouring of syrup in the column, and to investigate their formation mechanisms, we performed some experiments injecting single gas slugs in bubble-free glucose syrup (which had been left to degas in the column for several weeks). During the experiments, small bubbles formed both from the top of the column during the burst of gas slugs (as already described by *Pandit et al.* [1987], *Bird et al.* [2010], and *Seyfried and Freundt* [2000]) and within the inner portion during coalescence of two consecutive gas slugs, due to the collapse of partially resorbed liquid film on the bottom of the newly formed bubble.

[28] Coalescence between gas slugs typically occurs due to entrainment phenomena [*Manga and Stone*, 1994] or wake effects [*De Nevers and Wu*, 1971; *Bhaga and Weber*, 1981; *Colella et al.*, 1999]. This was also observed in our experiments. Interaction among small bubbles at the conduit walls was strongly affected by shearing; coalescence occurred mainly between large bubbles and was negligible between smaller, spherical bubbles (diameter ≤1 mm). We observed two main mechanisms for bubble coalescence, suggesting that it was mostly controlled by buoyancy and shearing: (1) a large (centimeter size) bubble, decoupled from the liquid, intersects a smaller one with lower velocity and the horizontal film between them is rapidly resorbed; (2) two elongated bubbles come in contact during liquid shearing at the walls related to the passage of the gas slug. Coalescence occurs at the surface that is parallel to the shearing direction.

[29] In experiments starting with bubble-free syrup, the number of small bubbles was observed to increase with time until stationary conditions were attained and a stable population characterized each gas volume flow rate. An example of spatial distribution of small bubbles as seen from the pipe walls, calculated by processing random images captured during a run at u_{sg} = 0.06 m/s, is shown in Figure 4. Their average dimension decreased with increasing superficial gas velocity, ranging from centimeter to submillimeter size, due to increasing shearing-induced breakup in the liquid film at the pipe walls. After all the experiments, submillimeter bubbles remained trapped in the glucose syrup for several weeks to months. Their concentration was calculated measuring the density of the bubbly liquid at the beginning of any new set of experiments, and their contribution was considered in calculating the average gas volume fraction.

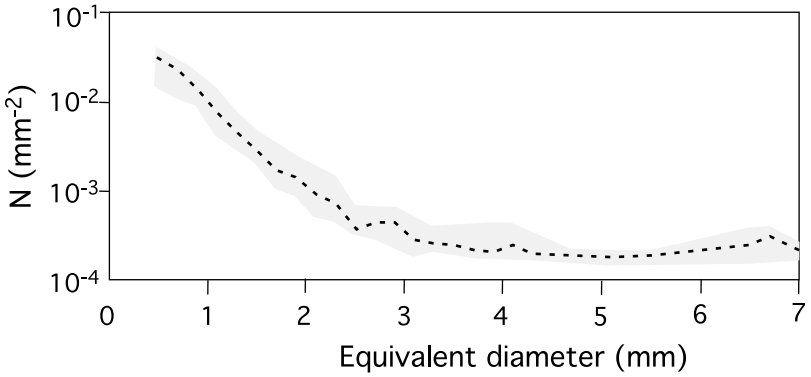

Figure 4. Areal bubble size distribution as observed at the pipe wall during a syrup-air, 5 min long, experiment with gas superficial velocity of 0.06 m/s calculated from a series of five images taken at random intervals. The gray area represents the total distribution variability, and the dashed line is the average value. The images were selected at random from a high-definition (8.9 pixels per mm), 25 fps movie of the run. 850 to 500 bubbles were analyzed in each image through standard image analysis techniques.

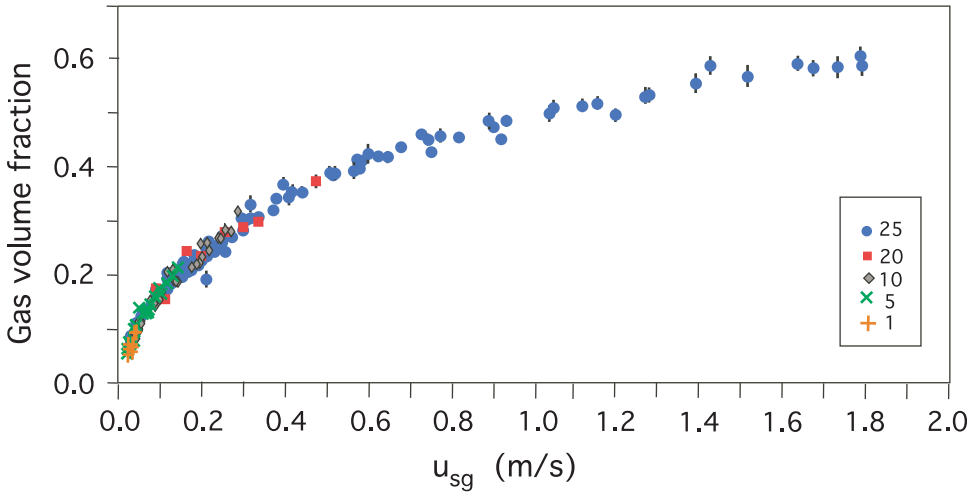

Figure 5. Gas volume fraction variations with superficial gas velocity (u_{sg}) for water-air experiments. Numbers in the legend indicate the number of active nozzles used to inject gas. Vertical error bars indicate variability of gas fraction calculated for maximum and minimum column height during fluctuations at equilibrium. Horizontal dimension of circles is larger than the expected error in determination of u_{sg}.

3.2. Average Volume Gas Fraction

[30] The experiments showed a progressive increase of the average volumetric gas content ε_g of the column with increasing gas flux, and no dependence on the initial bubble size (which varied with gas superficial velocity and the number of active nozzles) and the column height, suggesting that stationary conditions were reached during all the experiments (Figures 5 and 6). Pure syrup-air experiments show a higher dispersion at high superficial gas velocities (churn flow conditions), which is probably related to a less accurate estimation of the average column height due to larger and faster oscillations.

[31] For all liquids, the curves show an asymptotic behavior toward high superficial gas velocities. This pattern marks the transition to churn flow regimes when the bubbly column approaches the gas volume fraction typical for annular flow conditions, which is the maximum value that can be attained before onset of dispersed flow. Our experiments suggest that this transition occurs at lower superficial gas velocities with increasing liquid viscosity. This means that for low superficial gas velocities, higher viscosity liquids can attain the highest gas volume fraction, whereas for high superficial gas velocities, lower liquid viscosity shows the higher gas volume fraction. In fact, higher gas fractions are expected under annular flow conditions for lower viscosity liquids, due to smaller thickness of the liquid film at the pipe walls, which is a power law function of the liquid film Reynolds number [*Asali et al.*, 1985].

[32] The initial amount of small bubbles dispersed in the syrup and mixtures (ranging from 2 to 6 vol. %, marked on Figure 6 as points at zero u_{sg}) does not affect the gas volume fraction pattern, suggesting that equilibrium dynamics was not significantly affected by initial conditions. This observation is also confirmed by the lack of any relevant hysteretic effects; the average gas fraction was measured for two consecutive series of experiments with increasing and decreasing gas fluxes, respectively, and the results indicate no significant variations at corresponding superficial gas velocities.

3.3. Pressure Gradient

[33] Pressure gradients were computed from the instantaneous pressure data from two different sensors. In general, the time-averaged pressure gradient in the column decreases with increasing gas flux because of the reduced density of the mixture, but the amplitude of their oscillations increase (Figure 7), down to a minimum value, corresponding to the plateau in the u_{sg}/volume gas fraction plot. The pressure gradient is controlled by both liquid density and viscosity. At low gas superficial velocities, the gradient is higher for air-pure syrup or air-mixture experiments than for water-air experiments. It decreases more rapidly with increasing u_{sg}

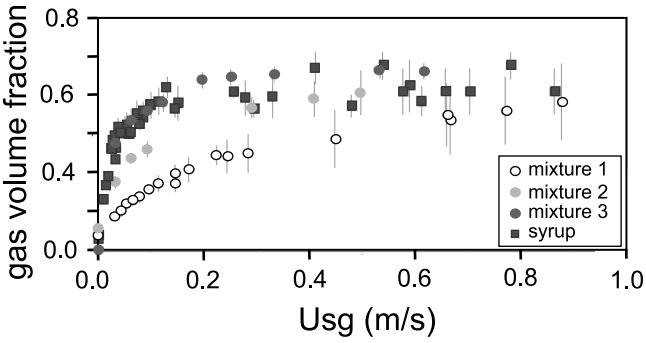

Figure 6. Gas volume fraction variation for different superficial gas velocities (u_{sg}). Error bars indicate gas fraction calculated for maximum and minimum column height during fluctuations at equilibrium. Horizontal dimension of circles and squares is larger than the expected error in determination of u_{sg}. The legend indicates the liquid used, whose characteristics are listed in Table 1. Horizontal dimension of symbols is larger than the expected error in determination of u_{sg}.

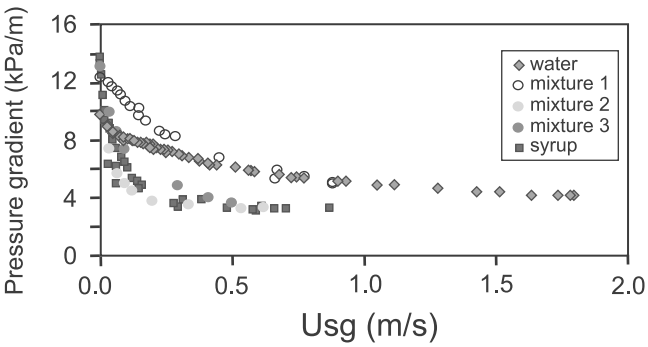

Figure 7. Pressure gradient variations with u_{sg} for the two-phase flow experiments. The legend indicates the liquid used, whose characteristics are listed in Table 1. Horizontal dimension of symbols is larger than the expected error in determination of u_{sg}.

in flows with higher viscosity liquids, reaching lower values for syrup and mixtures than the water experiments. For higher superficial gas velocities (churn flow conditions) the gradient has minimal variations for increasing gas fluxes, and curves show an asymptotic trend to a minimum pressure gradient.

4. Data Modeling

4.1. Column Gas Fraction

[34] The variation of the gas volume fraction ε_g of a bubble column is a complex function of several variables:

$$\varepsilon_g = f(\rho_l, \rho_g, D_p, d_b, \sigma, \eta_l, u_{sg}, u_{sl}) \tag{6}$$

where ρ_l and ρ_g are the liquid and gas densities, respectively, σ is the liquid surface tension, η_l is the liquid viscosity. The gas fraction can change within the column due to gas expansion (with changes gas density and superficial gas velocity) and progressive coalescence of gas bubbles.

[35] Several relationships have been developed based on experimental data, most of which cannot be directly applied to our experiments (and magmatic flows in conduits) because of significant scaling issues as none of the experiments reproduced large conduits and high viscosity liquid-gas flow dynamics (as described in the review paper of *Woldesemayat and Ghajar* [2007]). In order to model gas fraction variations, a more rigorous physical approach is needed. Under stationary conditions, and accounting for separated flow effects, the gas volume fraction is a function of gas volumetric flux Q_g and gas velocity u_g [*Behringer*, 1936]:

$$\varepsilon_g = \frac{Q_g}{A \cdot u_g} = \frac{u_{gs}}{u_g}. \tag{7}$$

The gas velocity is given by the contributions of the mixture velocity and the drift velocity v_{gd}, which is the rise velocity of the gas bubbles within the liquid (i.e., the terminal rise velocity of a single bubble) [*Zuber and Findlay*, 1965; *Wallis*, 1969].

[36] For heterogeneous flow conditions (defined as when the flow consists of bubbles with a range of sizes and all interact), this relation can be rewritten in more general terms [*Wallis*, 1969; *Ruzicka et al.*, 2001]:

$$\varepsilon_g = \frac{u_{sg}}{C_0 \cdot u_{sg} + v_{gd}} \tag{8}$$

where C_0 is the distribution parameter, a constant related to the shape of the axial profile of velocity in the conduit (*Zuber and Findlay* [1965], also discussed in the work of *Pioli et al.* [2009]). In turbulent flows, C_0 varies with Reynolds and Eotvos numbers and has a value between 1.2 and 1.4 [*Collins et al.*, 1978; *Fabre and Liné*, 1992; *Viana et al.*, 2003]; whereas for laminar flows it varies with conduit Eotvos number only according to the law derived by *Bendiksen* [1985]:

$$C_0 = 2.29\left[1 - \frac{20}{Eo}\left(1 - e^{-0.0125Eo}\right)\right] \tag{9}$$

C_0 can also be estimated from experiments noting that for high gas volume fluxes, the gas volume fraction of the column approaches an asymptotic value because [*Wallis*, 1969]:

$$(1 - C_0\varepsilon_g) \rightarrow 0 \tag{10}$$

so

$$\varepsilon_{g,\max} = \frac{1}{C_0} \tag{11}$$

where $\varepsilon_{g,\max}$ is the asymptotic gas fraction value. For pure syrup, experimental results indicate that $C_0 \sim 2.29$ in agreement with the theoretical prediction (equation (9)), whereas for water $C_0 = 1.4$.

[37] For bubbly flows of low viscosity liquids (0.001 Pa s), it has been suggested that the terminal bubble velocity (gas drift velocity) can be described by

$$v_{gd} = K\left(\frac{\sigma\ g(\rho_l - \rho_g)}{\rho_l^2}\right)^{0.25} \tag{12}$$

with $K_1 = 1.53$ [*Harmathy*, 1960]. For more viscous liquids, a lower value of K_1 has been suggested. For slug flow the drift velocity of a bubble is proportional to the square root of the pipe diameter D [*White and Beardmore*, 1962]:

$$v_{gd} = Fr\sqrt{gD_p}. \tag{13}$$

For water-air experiments, the regime is inertia-dominant ($N_f > 300$ and $Eo > 10^2$ which suggests that viscosity and surface tension effects can be neglected), and the Froude number is taken to have a value of 0.351 [*Wallis*, 1969]. In general, the Froude number can be expressed as a complex function of Eotvos and Reynolds number. Using the model proposed by *Viana et al.* [2003], we calculated the expected Froude number for our glucose syrup-air experiments of 0.23.

4.2. Pressure Drop in the Column

[38] Vertical pressure variations in the column can be calculated from the momentum equation. In the case of

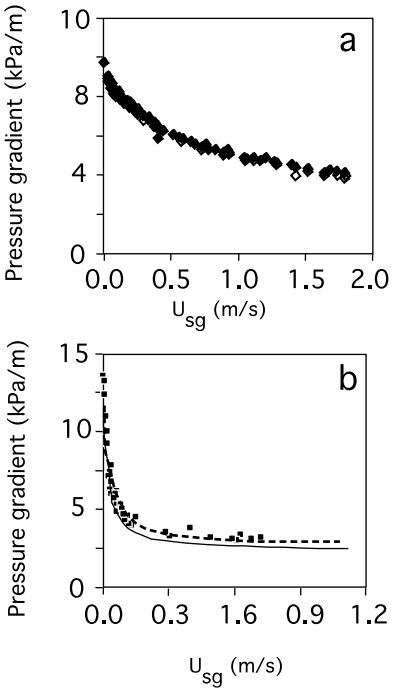

Figure 8. Comparison between theoretical and experimental pressure gradient variation with superficial gas velocity. (a) Water-air experiment, where black diamonds represent experimental results and white diamonds represent gravitational component as calculated from average gas fraction of the column for water-air experiments, and (b) pure syrup-air experiments. Squares represent experimental pressure gradient; solid line represents theoretical gradient for slug flow, calculated assuming no microvesicularity in the liquid; and dashed line is the best fit gradient, which assumes microvesicularity of the liquid of 10 vol. %.

steady flow, adopting cylindrical coordinates, the pressure variation can be simplified to the sum of the gravitational (G), friction (F), and acceleration (A) components [*Wallis*, 1969, p. 19]:

$$-\frac{dp}{dz} = -\frac{dp_G}{dz} - \frac{dp_F}{dz} - \frac{dp_A}{dz} \tag{14}$$

which, for bubbly flows, can be rewritten as [*Whalley*, 1986]

$$-\frac{dp}{dz} = \left[\varepsilon_g \rho_g + (1-\varepsilon_g)\rho_l\right] \cdot g + \frac{4\tau}{d} + G^2 \frac{d}{dz}\left(\frac{x^2}{\varepsilon_g \rho_g} + \frac{(1-x)^2}{(1-\varepsilon_g)\rho_l}\right) \tag{15}$$

where the three terms on the right-hand side of the equation correspond to gravitational, friction, and acceleration contributions, respectively, and τ is the shear stress, G is the total mass flux, and x is the flow quality, i.e., the mass fraction of the flow rate which is gas. The total pressure drop can be calculated neglecting the acceleration component (which can be considered a valid assumption since the liquid ouflux is zero, $x = 1$) and calculating the friction component for a bubble column following *Guet and Ooms* [2006]:

$$p_2(h) = \int_0^h \left(\left(\varepsilon_g \rho_g + (1-\varepsilon_g)\rho_l\right) g + \frac{\left(\varepsilon_g \rho_g + (1-\varepsilon_g)\rho_l\right)}{2D} f_m u_{sg}^2 \right) dz \tag{16}$$

where f_m is the Darcy friction factor, which is a dimensionless coefficient relating the friction pressure loss to the volumetric flow rate, and equals 64/Re for laminar flows [*Moody*, 1944].

[39] In water-air experiments, the measured pressure drop is coincident with the gravitational pressure drop as calculated from the average gas volume fraction and the friction component can be neglected (Figure 8a).

[40] In slug flows, and therefore in our all syrup experiments, the gravitational component depends on the fractional slug length β which is the ratio between the length of the gas slug and the total length of the slug unit (comprising the gas slug and the liquid between two consecutive slugs), and the acceleration component can be neglected because it represents only a small contribution when the liquid flow is zero [*De Cachard and Delhaye*, 1996]. The total pressure drop reduces to

$$-\frac{dp_G}{dz} - \frac{dp_F}{dz} = (1-\beta)\rho_l g \left[1 + \frac{f_m u_{sg}^2}{2gD}\right]. \tag{17}$$

The fractional slug length can be calculated for any superficial gas velocity solving a system of equations as shown in Appendix A. As before, the second term in the square brackets of the equation (17) can be neglected because of the low range of superficial gas velocities (Figure 8b). Moreover, using the model described above, the experimental data are best reproduced assuming a volume concentration of small bubbles in the liquid matrix of 0.10 (Figure 8b). This value is in good agreement with the volume percentage of bubbles calculated from the density of the bubbly liquid at the end of the experiments, which varied from 6 to 2 vol. %, measured a few hours to a few weeks after the experiments, respectively.

5. Application to Magmatic Systems

5.1. Expected Conditions for Degassing of Basaltic Magmas

[41] Using the models described here, it is possible to infer the properties of a degassing column of stagnant basaltic magma for a range of conditions. To calculate gas fraction volume variations with the gas flux, it is necessary to estimate a value for the main coefficients: the distribution parameter C_0, which controls the maximum vesicularity of the column (and the thickness of the annular film) and the Froude number, which controls the rise velocity of gas slugs and the stability of slug flow. As none of these numbers have been directly measured for magmas, they must be estimated

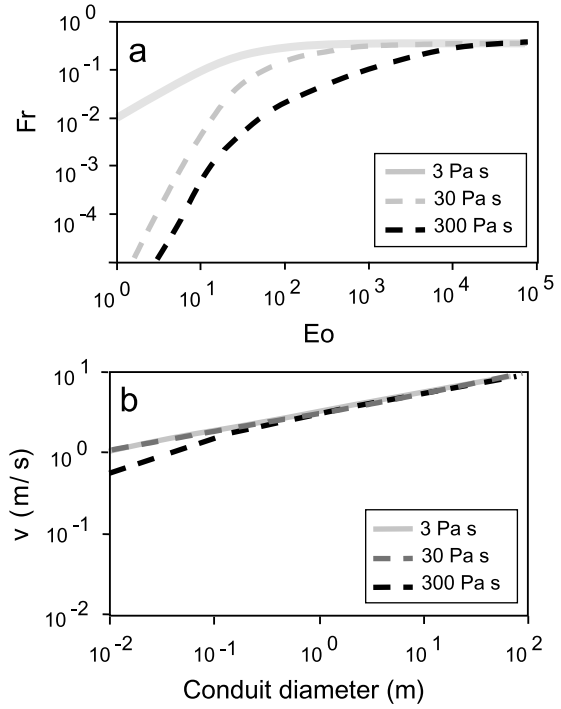

Figure 9. (a) Variation of Froude number (*Fr*) with conduit Eotvos number (*Eo*) and (b) expected rise velocity of gas slugs as a function of conduit diameter for basaltic magmas with different viscosities.

using more general models. C_0, as calculated from equation (9), is expected to have a value of approximately 2.29, whereas the Froude number is expected to change with magma viscosity and conduit diameter (Figures 9a and 9b) according to the experimental model proposed by *Viana et al.* [2003] basing on a wide data set on the rise of gas slugs within different liquids. This model computes the Froude number as a power law function of the Eotvos and buoyancy Reynolds number (*R*) and considers the contribution of inertial, viscous, and interfacial forces for a wide ranges of dynamic regimes.

[42] The variations of magma average vesicularity for a range of conditions are estimated in Figure 10a; the vesicularity of the magma increases with increasing superficial gas velocity, reaching a maximum value of ~0.45, corresponding to the expected conditions for annular flow. An increase in viscosity of the magma increases the vesicularity of the mixture at low superficial gas velocities and decreases the stability of slug flow, favoring churn flow conditions, above which, higher vesicularities are expected for lower viscosities basaltic magmas. This can be explained with an increased coalescence efficiency, which favors formation of large bubbles and flooding. Also, the *Bendiksen* [1985] and *Viana et al.* [2003] models suggest that conduit diameter controls both the Froude number and C_0, decreasing the expected vesicularity for the formation of large vesicles in the conduit and the volume of gas required. These results suggest that when the conditions for separated two-phase flow are met, an increase in viscosity of the magma will favor bubble coalescence and increase the bubble size in the mixture. Also, with increasing conduit diameter, the effect of viscosity becomes less important and magmas with different viscosities show similar degassing dynamics. Figure 10a suggests that transition to annular flow (which is indicated by the asymptotic behavior in the vesicularity-superficial gas velocity curve) occurs at superficial gas velocities, which increase with increasing conduit diameter and decreasing magma viscosity. In terms of volcanic activity, transition to annular flow should determine the onset of gas-driven eruptions, as the liquid is dragged upward by the gas.

[43] A more precise quantification of the threshold gas flow rate for the onset of annular flow dynamics was done by *Zapke and Kröger* [1996, 2000] which, based on experimental data, proposed that the threshold u_{sg} is a function of the Ohnesorge number $Oh = \eta_l/(D\,\rho_l\,\sigma)^{0.5}$ [*Ohnesorge*, 1936], which relates viscous forces to inertial and surface tension forces and the densimetric gas Froude number $Fr_{HG} = Fr\,\rho_g/(\rho_l-\rho_g)$. When applying this model to magma, we find that the threshold u_{sg} ranges from ~28 m/s (2×10^4 m^3/s) (D = 1 m, η_l = 300 Pa s) to 156 m/s (1×10^3 m^3/s) (D = 10 m, η_l = 300 Pa s). These values (from 8.6×10^7 to 1.7×10^9 m^3/day can be considered unrealistic in passive degassing conditions at central conduits [*Ripepe et al.*, 2002, 2008; *McGonigle et al.*, 2003; *Aiuppa et al.*, 2008; *Boichu et al.*, 2010; *Sawyer et al.*, 2008], and more typical of eruptive events.

[44] The pressure gradients expected for magmatic columns strongly depend on the flow regime. In fact, if the maximum stable bubble diameter is smaller than the conduit, no continuous slug flow is possible and the pressure gradient

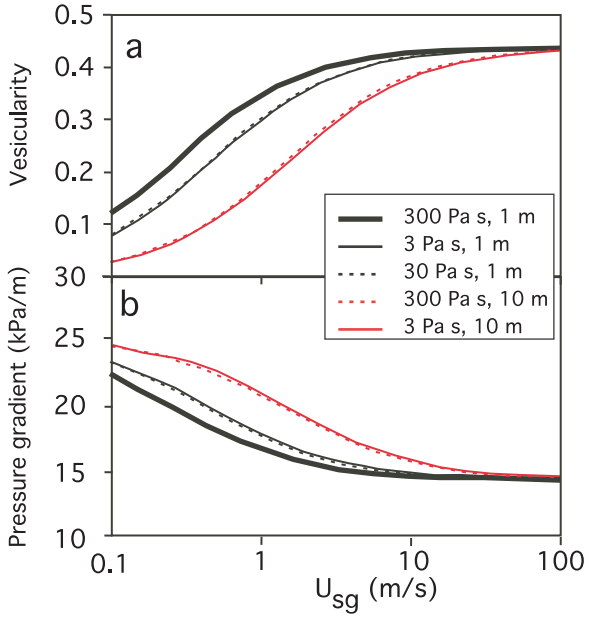

Figure 10. (a) Expected vesicularity of a degassing magma column with increasing superficial gas velocity. Values indicate viscosity (Pa s) and conduit diameter (m). (b) Expected shallow pressure gradient for magma flow in a circular conduit. Bubbly to churn flow conditions. Thick black solid line represents ρ_l = 300 Pa s, *D* = 1 m; thin black solid line represents ρ_l = 3 Pa s, *D* = 1 m; black dashed line represents ρ_l = 30 Pa s, *D* = 1 m; red dashed line represents ρ_l = 3 Pa s, *D* = 10 m; and red solid line represents ρ_l = 300 Pa s, *D* = 10 m.

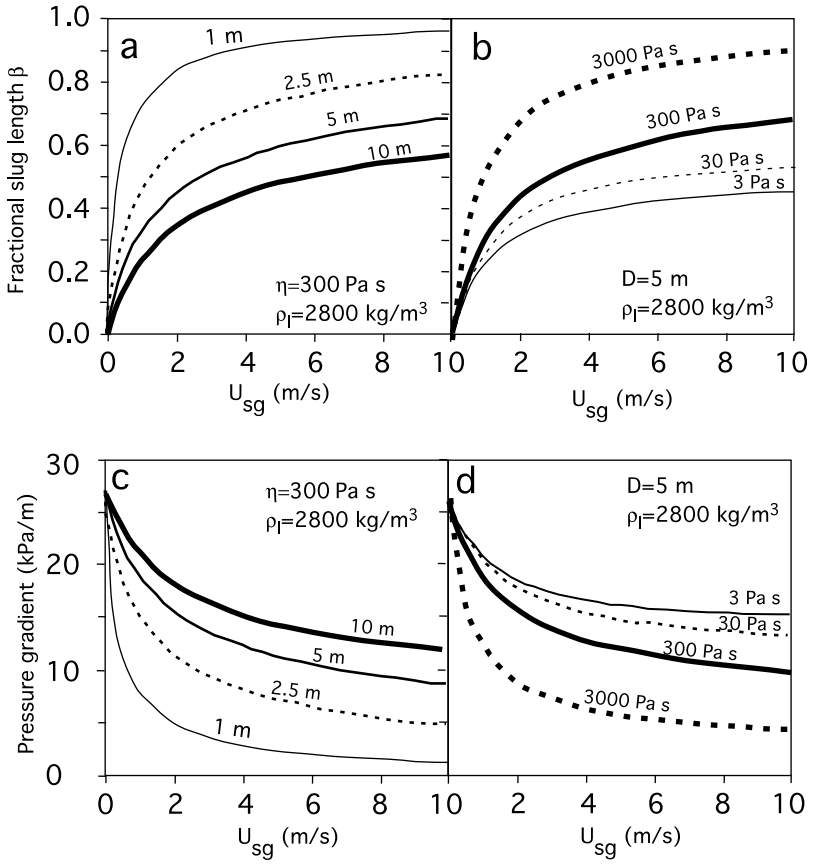

Figure 11. Variation of fractional slug length in a degassing magma column with (a) conduit diameter and (b) magma viscosity. Variation of the pressure gradient with (c) conduit diameter and (d) magma viscosity.

is a direct function of the magma average vesicularity (Figure 10b), but if the conditions for stable slug flow are met, the pressure gradient depends on the fractional slug length β and for similar gas flow rates, lower values are expected (Figure 11). Considering both our direct observations and previous studies (mentioned in section 1.2), we can hypothesize that stable slug flow conditions (i.e., when, at constant flow rates, the gas rises as a continuous sequence of equally spaced slugs) are very likely to be met in small conduits (with D up to a few m) and unlikely for low viscosity (a few to some tens of Pa s) magmas degassing in large conduits (with diameters of 10 to a few tens of meters). Stable slug flow requires noncontinuous, but regular, gas supply at the base of the conduit. These observations do not exclude the possibility of the rise of a single gas slug within a stagnant liquid, which can been experimentally reproduced within large diameters pipes even for very low viscosity liquids (i.e., within water, along a 0.24 m diameter pipe [*James et al.*, 2011]). Moreover, it is important to remember that our experiments did not test the validity of these models for very large diameters and they should be considered only a first-order approximation until full validation.

[45] When extrapolating the gradient to depth, it is necessary to take into account gas volume changes due to pressure variations, and their effect on the volume gas flow rate (and superficial gas velocity), as already suggested by *James et al.* [2008]. As the model does not consider the effects of gas exsolution and diffusion, we limit the calculations to a hundred meters below the surface. We assume isothermal expansion and mass conservation to calculate changes in the gas superficial velocity up the column. As an example, we computed the expected pressure variation in a degassing conduit fixing gas superficial velocity at the vent at atmospheric pressure. Superficial velocities at different depths, and hence different pressures were calculated in a stepwise approach. The approach was implemented using small step lengths (1 m). Results are shown in Figure 12 where the nonlinear trends in the curves show the gas expansion effects. In this it was assumed that the conditions for slug flow stability are met. The additional, near surface expansion dynamics demonstrated by *James et al.* [2008, 2009] were not taken into account.

5.2. Scale of Gas Transport Structures and Formation of Small Bubbles

[46] The bubble size distribution within a degassing magma column derives from the balance of coalescence and breakup phenomena. Coalescence is a dynamic process depending not only on bubble size and magma properties but also on the vertical and lateral velocity distribution within the column. The breakup rate in magmatic flows is expected to be very low, due to complete suppression of turbulence phenomena, and is dominated by bubble instability. In the case of a homogenous population of small bubbles, the flow

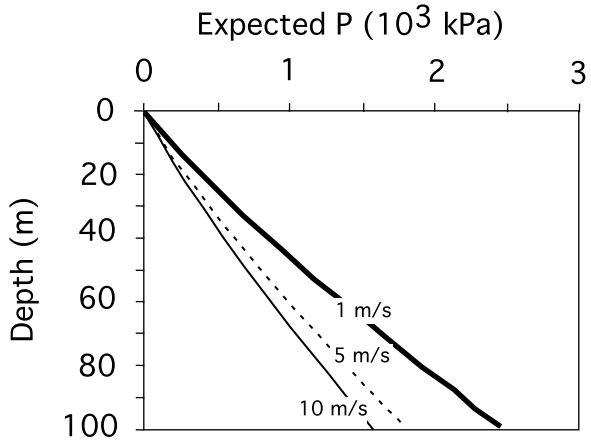

Figure 12. Expected pressure variations in a degassing magma column for gas superficial velocities of 1, 5, 10 m/s measured at the vent; conduit diameter of 5 m and magma viscosity of 300 Pa s; and magma density of 2600 kg/m^3.

field is laminar with no lateral gradient and the collision frequency is very low. In this case, disturbance of the flow field generated by geometric irregularities within the conduit might play a role in coalescence phenomena at depth [*Seyfried and Freundt*, 2000]. The larger the bubble size distribution, the larger the variation in bubble rise speed and shearing effects, and the more important are the dynamic effects. Moreover, coalescence phenomena are more effective for larger bubbles because, due to their wide surfaces, they display larger contact areas and higher characteristic contact times during collisions and hence higher collision efficiency [*Prince and Blanch*, 1990]. This phenomenon explains the reduced stability of bubbly flow in our glucose syrup experiments. Nonetheless, in a very long pipe, even at very small collision rates, coalescence of small bubbles can be effective and lead to a very narrow bubble size distribution, which is controlled by the largest stable bubble diameter. Our experiments showed, however, that a population of small bubbles is continuously formed as a result of both coalescence of large bubbles and bubble breakup at the top of the liquid free surface. The bubble size distribution is bimodal, consisting of (1) large bubbles (up to conduit size when stable) that rise rapidly through the liquid dominating outgassing and (2) small "matrix" bubbles which are unable to move within the liquid and recirculate with it. Small "matrix" bubbles do not play an important role in outgassing.

[47] Experimental results on two-phase flows with intermediate viscosity (a few Pa s) liquids suggest that the contribution of small bubbles to gas transport is between 20 and 50% of the total mass outflux [*Muller and Davidson*, 1992] and decreases with increasing superficial gas velocity. Since an increase of viscosity increases the stability of large bubbles, we suggest that the contribution of small bubbles to magma outgassing should be considerably lower with respect to large (decimeter to meter sized) bubbles.

5.3. Liquid Convection and Mixing

[48] The rise of bubbles is responsible for the formation of liquid circulation cells at the pipe wall. The size of the cells and their number increases with the bubble size and frequency. The circulation occurs both in bubbly and slug flow regimes. The motion ensures complete mixing and homogenization of the liquid, as suggested in our experiments by the homogeneous distribution of very small bubbles generated by bursting at the conduit top or by coalescence if gas slugs along the entire pipe height. These results suggest that gas flow circulation inside the conduit is likely responsible for continuous mixing of basaltic magma and can counteract the effect of cooling gradients resulting in more homogeneous magma composition and physical properties. This mechanism is different from the convection process driven by density differences, induced by degassing of a volatile-rich, rising magma batch [*Kazahaya et al.*, 2004; *Stevenson and Blake*, 1998].

[49] As our experiments did not reproduce the effect of magma cooling and crystallization and the formation of thermal gradients within the pipe, more dedicated studies are necessary to quantify the efficiency of liquid mixing for a range of gas flow rates. However, the effect of viscosity on pressure gradient, even over two orders of magnitude, is much lower than the effect of gas flow rate. This implies that the effects of these processes (which would affect liquid viscosity) on pressure profiles might not be large.

6. Conclusions

[50] The physical characteristics (vesicularity, pressure gradient, and flow geometry) of the shallow portion of a degassing magma column have been investigated combining drift flux theory and analogue experiments. The experiments could reproduce only magma outgassing conditions, and the model we used to calculate the expected properties of the magma column does not take into account the contribution of the liquid outflow on the flow dynamics. However, regime transitions and the characteristic of large-scale liquid circulation are expected to occur in hydrodynamic similarity (i.e., the velocity profile and the liquid recirculation patterns inside the column coincide for flows with different u_{sl} when the column gas volume fractions are the same) during eruptive processes (when the magma rise velocity is >0, but considerably lower than the gas flux). In particular, flow pattern transitions are expected to be shifted at higher superficial gas velocities for $u_{sl} > 0$ [*Mudde and Saito*, 2001].

[51] Our experimental results also suggest a direct relationship between the superficial gas velocity and all the properties of the magmatic mixture. The average vesicularity of the magma increases with increasing superficial gas velocity, determining a progressive decrease in the pressure gradient. It is also affected by the physical and rheological properties of the magma. The theoretical model predicts that for the same superficial gas velocity, it increases with decreasing conduit diameters and with increasing magma viscosity (this aspect is also confirmed by the experiments). The maximum vesicularity attained by magma, corresponding to churn and annular flow regimes, changes with the Eotvos number (equation (9)) and is expected to be around 0.45. The pressure gradient in the magmatic column also decreases with increasing superficial gas velocity, with increasing magma viscosity and with decreasing conduit diameter.

[52] The high viscosity of magma suppresses turbulence and promotes bubble coalescence, with formation of large

bubbles, also favored by large L/D ratios, which are expected in natural systems. Degassing processes also determine the formation of circulation cells within the conduit and continuous mixing, favoring magma homogeneity.

[53] Our experiments suggest that the bubble size distribution in the flow is not controlled only by bubble interaction processes, but the coalescence of large bubbles and their breakup at the magma free surface is forming a stable population of smaller bubbles, deriving from incomplete collapse of bubble ruptured films. These bubbles are too small to move within the liquid and circulate with it. They are also not significantly contributing to outgassing. It is interesting to note the occurrence of small bubbles during stable slug flow and liquid mixing was already noticed in the experiments of *Seyfried and Freundt* [2000], which used water-salt solutions (viscosities comprised between 10^0 and 10^1 mPa s) and air. We observe, however, that most of these small bubbles likely originated in the wakes behind the gas slugs due to the low viscosity of the liquid used and not necessarily only by air trapping during the bubbles burst. In any case, they observed that for continuous gas supply, the bubbles rapidly distributed along the entire column due to backflow in the liquid.

[54] These observations suggest that more specific studies are necessary to evaluate the significance of the vesicularity and texture of scoria samples erupted during low explosivity (Strombolian) regimes where gas segregation processes are of primary importance. In particular, the permeability of degassing magma should be controlled by large-scale structures and not by the microscale bubble distribution that reflects the bubble content of small parcels of magma and is controlled by the dynamics of the liquid motions.

[55] Annular flow conditions are unlikely to be met unless the conduit diameter is very small (a few meters).

Appendix A: Calculation of Fractional Slug Length

[56] The fractional slug length $\beta = l_{TB}/l$ is the ratio between the length of the gas slug (l_{TB}) and the total length of the slug unit (l), which also comprises the liquid separating two consecutive bubbles (Figure A1). *Fernandes et al.* [1983] introduced this parameter in a general model describing the hydrodynamics of slug flow. To calculate β, we adapt and solve simultaneously a system of equations derived from their model.

[57] The average gas volume fraction in the slug unit can be considered equal to the average gas fraction in the entire column. It is also equal to the sum of the gas volume fraction in the gas slug area (ε_{TB}) and the gas volume fraction in the in the liquid between two consecutive gas slugs (ε_{LS}) multiplied by their relative lengths:

$$\varepsilon_g = \beta\varepsilon_{TB} + (1-\beta)\varepsilon_{LS}. \tag{A1}$$

Mass balance requires that the superficial gas velocity equals the sum of the average velocity of the gas in the slug (u_{GTB}) and the average velocity of the small bubbles in the liquid between two consecutive gas slugs (u_{GLS}):

$$u_{gs} = \beta\varepsilon_{TB}u_{GTB} + (1-\beta)\varepsilon_{LS}u_{GLS}. \tag{A2}$$

Also, the net liquid velocity is zero, then:

$$(1-\beta)(1-\varepsilon_{LS})u_{LLS} - \beta(1-\varepsilon_{TB})u_{LTB} = 0 \tag{A3}$$

where u_{LLS} is the velocity of liquid in between two gas slugs and u_{LTB} is the velocity of the liquid in the film around the gas slugs.

[58] At equilibrium conditions, the continuity equations for liquid and gas are

$$(1-\varepsilon_{LS})\left(u_g - u_{LLS}\right) = (1-\varepsilon_{TB})\left(u_g - u_{LTB}\right) \tag{A4}$$

$$\varepsilon_{LS}\left(u_g - u_{GLS}\right) = \varepsilon_{TB}\left(u_g - u_{GTB}\right), \tag{A5}$$

respectively.

[59] The rise velocity of the small bubbles in the liquid between two consecutive gas slugs can be calculated after *Harmathy* [1960] and *Zuber and Hench* [1962]:

$$u_{GLS} = u_{LLS} + K_1\left(\frac{\sigma g\left(\rho_l - \rho_g\right)}{\rho_l^2}\right)^{0.25}(1-\varepsilon_{LS})^{0.5}. \tag{A6}$$

Finally, the downward velocity of the liquid in the film around gas slugs was calculated by *De Cachard and Delhaye* [1996], basing on the thickness of the film as modeled by *Wallis* [1969] and *Nusselt* [1916]:

$$V_{LTB} = -11.2\left[gD\left(1-\varepsilon_{TB}^{0.5}\right)\right]^{0.5} \tag{A7}$$

that is valid for turbulent regimes, and

$$u_{LTB} = -0.333\left(\frac{g\rho_l D^2}{\eta_l}\right)\left(1-\varepsilon_{TB}^2\right)^2 \tag{A8}$$

for laminar regimes.

[60] As explained in section 4.2, the rise velocity of gas u_g is

$$u_g = C_0 u_{sg} + Fr\sqrt{gD}. \tag{A9}$$

There are in total seven variables, β, ε_{TB}, ε_{LS}, u_{GTB}, u_{GLS}, u_{LLS}, u_{LTB} which can be calculated solving simultaneously equations from (A1) to (A7) or (A8) and calculating the gas velocity from equation (A9).

Notation

A	pipe cross-section area (m^2).
C_0	distribution parameter.
D	pipe diameter (m).
d_b	bubble diameter (m).
$d_{b,max}$	maximum stable bubble diameter (m).
f_m	friction factor.
G	mass flow rate (kg/s).
G_g	gas mass flow rate (kg/s).
L	pipe length (m).
Q_g	gas volume flux (m/s).
t_{ij}	coalescence time between bubbles of diameter i and j (s).

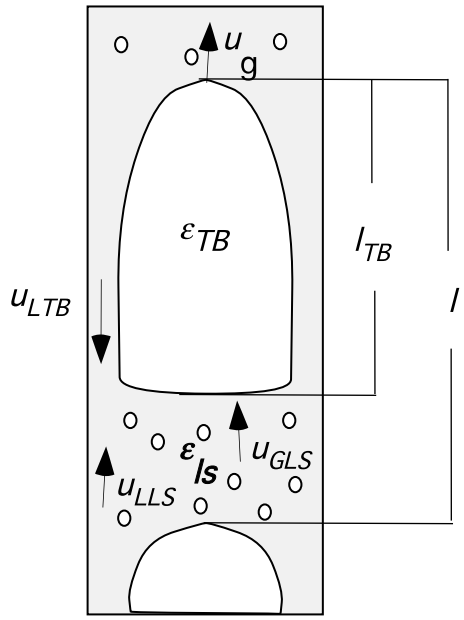

Figure A1. Schematic section of a slug unit.

T_{ij} bubble contact time between bubbles of sizes i and j (s).
u_g gas velocity (m/s).
u_{GTB} average velocity of the gas in the slug (m/s).
u_{GLS} average velocity of the small bubbles in the liquid between two consecutive gas slugs (m/s).
u_{LLS} velocity of liquid in between two gas slugs (m/s).
u_{LTB} velocity of the liquid in the film around the gas slugs (m/s).
u_l liquid velocity (m/s).
u_{sg} superficial gas velocity (m/s).
u_{sl} superficial liquid velocity (m/s).
v_{gd} gas drift velocity (m/s).
V_m mixture velocity (m/s).
x flow quality = G_g/G.
β fractional slug length.
Γ bubble coalescence rate ($1/m^3s$).
ε_g gas volume fraction.
ε_{TB} gas volume fraction in the gas slug volume.
ε_{LS} gas volume fraction in the liquid between two gas slugs.
η_l viscosity (Pa s).
Θ_{ij}^T, Θ_{ij}^B, Θ_{ij}^L collision frequency related to turbulence, buoyancy, laminar effects ($1/m^3s$).
ρ_g gas density (kg/m^3).
ρ_l liquid density (kg/m^3).
τ wall shear stress (Pa).
σ surface tension (N/m).
Eo Eotvos number = $g(\rho_l-\rho_g)d_b^2/\sigma$.
Fr Froude number = $v_{gd}/(gD)^{0.5}$.
Fr_{HG} densimetric gas Froude number = $(\rho_g u_{sg}^2)/[gD(\rho_l-\rho_g)]$.
Mo Morton number = $g\eta_l^4(\rho_l-\rho_g)/\rho_l^2\sigma^3$.
N_η dimensionless viscosity = $\eta_l (g\sigma/\rho_l)^{0.25}/\sigma$.
Oh Ohnesorge number = $\eta_l/(D\ \rho_l\ \sigma)^{0.5}$.
R Buoyancy Reynolds number = $(D^3\ g(\rho_l-\rho_g)\ \rho_l)^{0.5}/\eta$.
Re Reynolds number = $\rho_l\ d_b v/\eta$.
Re_f Reynolds number of the liquid film (in annular and slug flow).

[61] **Acknowledgments.** This work was supported by Fond National Suisse grants FNSF 200021–122268 and 200020–132543. J.P. was supported by the Natural Environment Research Council UK grants NE/G016593/1 and NE/F004222/1. The authors are grateful to P. Bennett and M. Hemsley for their precious support in building, setting up, and managing the experimental rig. O. Kajero is acknowledged for the viscosity measurements. The paper greatly improved after M. James and A. Clarke provided constructive and accurate reviews. The Editor, A. Revil, and the Associate Editor, Michael P. Ryan, are also acknowledged for the time and effort spent in managing and improving the paper.

References

Aiuppa, A., C. Federico, G. Giudice, S. Gurrieri, M. Liuzzo, H. Shinohara, R. Favara, and M. Valenza (2006), Rates of carbon dioxide plume degassing form Mount Etna volcano, *J. Geophys. Res.*, *111*, B09207, doi:10.1029/2006JB004307.

Aiuppa, A., G. Giudice, S. Gurrieri, M. Liuzzo, M. Burton, T. Caltabiano, A. McGonigle, G. Salerno, H. Shinohara, and M. Valenza (2008), Total volatile flux at Mount Etna, *Geophys. Res. Lett.*, *35*, L24302, doi:10.1029/2008GL035871.

Allard, P. J., N. Carbonelle, D. Dajlevic, J. Le Bronec, P. Morel, J. M. Maurenas, M. C. Robe, T. Faivre-Pierret, J. C. Sabroux, and P. Zettwog (1991), Eruptive diffuse emission of carbon dioxide from Etna volcano, *Nature*, *351*, 387–391.

Allard, P., J. Carbonelle, N. Métrich, H. Loyer, and P. Zettwoog (1994), Sulphur output and magma degassing budget of Stromboli volcano, *Nature*, *368*, 326–330, doi:10.1038/368326a0.

Allard, P., N. Métrich, and M. Burton (2002), Magma degassing and volatile budget at Mount Etna volcano, paper presented at the Chapman Conference on Volcanism and the Earth's Atmosphere, AGU, Thera, Greece.

Andronico, D., R. A. Corsaro, A. Cristaldi, and M. Polacci (2008), Characterizing high energy explosive eruptions at Stromboli volcano using multidisciplinary data: An example from the 9 January 2005 explosion, *J. Volcanol. Geotherm. Res.*, *176*, 541–550, doi:10.1016/j.jvolgeores.2008.05.011.

Asali, J. C., T. J. Hanratti, and P. Andreussi (1985), Interfacial drag and film height for vertical annular flow, *AIChE J.*, *31*, 895–902, doi:10.1002/aic.690310604.

Azzopardi, B. J., and E. Wren (2004), What is entrainment in vertical two-phase churn flow?, *Int. J. Multiphase Flow*, *30*, 89–103, doi:10.1016/j.ijmultiphaseflow.2003.11.001.

Barbosa, J. R., Jr., A. H. Govan, and G. F. Hewitt (2001), Visualisation and modelling studies of churn flow in a vertical pipe, *Int. J. Multiphase Flow*, *27*, 2105–2127, doi:10.1016/S0301-9322(01)00048-9.

Behringer, H. (1936), The flow of liquid-gas mixtures in vertical tubes, *Z. Gesamte Kalte Indust.*, *43*, 55–58.

Bendiksen, K. H. (1985), On the motion of long bubble sin vertical tubes, *Int. J. Multiphase Flow*, *11*, 797–812, doi:10.1016/0301-9322(85)90025-4.

Bhaga, D., and M. E. Weber (1981), Bubbles in viscous fluids: Shapes, wakes and velocities, *J. Fluid Mech.*, *105*, 61–85, doi:10.1017/S002211208100311X.

Bird, J. C., R. de Ruiter, L. Courbin, and H. A. Stone (2010), Daughter bubble cascade produced by folding of ruptured thin films, *Nature*, *465*, 759–762, doi:10.1038/nature09069.

Blackburn, E. A., L. Wilson, and R. J. S. Sparks (1976), Mechanisms and dynamics of Strombolian activity, *J. Geol. Soc.*, *132*, 429–440, doi:10.1144/gsjgs.132.4.0429.

Blower, J. D. (2001), Permeability-porosity relationships in magma, *Bull. Volcanol.*, *63*, 497–504, doi:10.1007/s004450100172.

Boichu, M., C. Oppenheimer, V. Tsanev, and P. R. Kyle (2010), High temporal resolution SO_2 flux measurements at Erebus volcano, Antarctica, *J. Volcanol. Geotherm. Res.*, *190*, 325–336, doi:10.1016/j.jvolgeores.2009.11.020.

Brown, R. A. S. (1965), The mechanics of large gas bubbles in tubes, *Can. J. Chem. Eng.*, *43*, 217–223, doi:10.1002/cjce.5450430501.

Burton, M. R., C. Oppenheimer, L. A. Hoorcks, and P. W. Francis (2000), Remote sensing of CO_2 and H_2O emission rates from Masaya volcano, Nicaragua, *Geology*, *28*, 915–918, doi:10.1130/0091-7613(2000)28<915:RSOCAH>2.0.CO;2.

Cheng, H., J. H. Hills, and B. J. Azzopardi (1998), A study of the bubble-to slug transition in vertical gas-liquid flow in columns of different diameter,

Int. J. Multiphase Flow, *24*, 431–452, doi:10.1016/S0301-9322(97)00067-0.

Cheng, H., J. H. Hills, and B. J. Azzopardi (2002), Effects of initial bubble size on flow pattern transition in a 28.9 mm diameter column, *Int. J. Multiphase Flow*, *28*, 1047–1062, doi:10.1016/S0301-9322(02)00013-7.

Clift, R., and J. R. Grace (1972), The mechanism of bubble breakup in fluidized beds, *Chem. Eng. Sci.*, *27*, 2309–2310, doi:10.1016/0009-2509(72)85111-X.

Clift, R., J. R. Grace, and M. E. Weber (1978), *Bubbles, Drops and Particles*, 380 pp., Academic, San Diego, Calif.

Colella, D., D. Vinci, R. Bagatin, M. Masi, and E. Abu Bakr (1999), A study on coalescence and breakage mechanisms in three different bubble columns, *Chem. Eng. Sci.*, *54*, 4767–4777, doi:10.1016/S0009-2509(99)00193-1.

Collins, R., F. F. de Moraes, J. F. Davidson, and D. Harrison (1978), The motion of large bubbles rising through liquid flowing in a tube, *J. Fluid Mech.*, *89*, 497–514, doi:10.1017/S0022112078002700.

Costigan, G., and P. B. Whalley (1997), Slug flow regime identification from dynamic void fraction measurements in vertical air-water flows, *Int. J. Multiphase Flow*, *23*, 263–282, doi:10.1016/S0301-9322(96)00050-X.

Davidson, J. F., and B. O. G. Schüler (1960), Bubble formation at an orifice in a viscous liquid, *Trans. Inst. Chem. Eng.*, *75*, suppl., S105–S115, doi:10.1016/S0263-8762(97)80008-1.

De Cachard, F., and J. M. Delhaye (1996), A slug-churn flow model for small-diameter airlift pumps, *Int. J. Multiphase Flow*, *22*, 627–649, doi:10.1016/0301-9322(96)00003-1.

Delnoij, E., J. A. M. Kuipers, and W. P. M. van Swaaij (1997), Dynamic simulation of gas-liquid two-phase flow: Effect of column aspect ratio on the flow structure, *Chem. Eng. Sci.*, *52*(21–22), 3759–3772, doi:10.1016/S0009-2509(97)00222-4.

De Nevers, N., and J.-L. Wu (1971), Bubble coalescence in viscous fluids, *AIChE J.*, *17*, 182–186, doi:10.1002/aic.690170136.

Edmonds, M., and T. M. Gerlach (2007), Vapor segregation and loss in basaltic melts, *Geology*, *35*, 751–754, doi:10.1130/G23464A.1.

Fabre, J., and A. Liné (1992), Modeling of two-phase slug flow, *Annu. Rev. Fluid Mech.*, *24*, 21–46, doi:10.1146/annurev.fl.24.010192.000321.

Fernandes, R. C., R. Semiat, and A. E. Dukler (1983), Hydrodynamic model for gas-liquid lug flow in vertical tubes, *AIChE J.*, *29*, 981–989, doi:10.1002/aic.690290617.

Gerlach, T. M., K. A. McGee, T. Elias, A. J. Sutton, and M. P. Doukas (2002), Carbon dioxide emission rate of Kilauea volcano: Implications for primary magma and the summit reservoir, *J. Geophys. Res.*, *107* (B9), 2189, doi:10.1029/2001JB000407.

Grevskott, S., B. H. Sannaes, M. P. Dudukovic, K. W. Hjarbo, and H. F. Svendsen (1996), Liquid circulation, bubble size distributions, and solid movement in two- and three- phase bubbles columns, *Chem. Eng. Sci.*, *51*(10), 1703–1713, doi:10.1016/0009-2509(96)00029-2.

Guedes de Carvalho, J. R. F., and M. J. Ferreira (2000), Pressure drop in gas slugs in vertical tubes and flooding instability, *AIChE J.*, *46*, 707–723, doi:10.1002/aic.690460406.

Guet, A., and G. Ooms (2006), Fluid mechanical aspects of the gas-lift technique, *Annu. Rev. Fluid Mech.*, *38*, 225–249.

Guet, S., G. Ooms, and R. V. A. Oliemans (2002), Influence of bubble size on the transition from low-Re bubbly flow to slug flow in a vertical pipe, *Exp. Therm. Fluid Sci.*, *26*, 635–641, doi:10.1016/S0894-1777(02)00172-3.

Harmathy, T. Z. (1960), Velocity of large drops and bubbles in media of infinite or restricted extent, *AIChE J.*, *6*, 281–288, doi:10.1002/aic.690060222.

Harris, A. J. L., and M. Ripepe (2007), Temperature and dynamics of degassing at Stromboli, *J. Geophys. Res.*, *112*, B03205, doi:10.1029/2006JB004393.

Hesketh, R. P., A. W. Etchells, and E. W. F. Russell (1991), Bubble breakage in pipeline flow, *Chem. Eng. Sci.*, *46*(1), 1–9, doi:10.1016/0009-2509(91)80110-K.

Hewitt, G. F., and N. S. Hall-Taylor (1970), *Annular Two-Phase Flow*, 310 pp., Pergamon, Oxford, U. K.

Hewitt, G. F., and D. N. Roberts (1969), Studies of two-phase patterns by simultaneous X-ray and flash photography, *Rep. AERE M2159*, At. Energy Res. Est., Harwell, U. K.

Hinze, J. O. (1955), Fundamentals of the hydrodynamic mechanism of splitting in dispersion processes, *AIChE J.*, *1*, 289–295, doi:10.1002/aic.690010303.

James, M. R., S. J. Lane, B. Chouet, and J. Gilbert (2004), Pressure changes associated with the ascent and bursting of gas slugs in liquid-filled vertical and inclined conduits, *J. Volcanol. Geotherm. Res.*, *129*(1–3), 61–82, doi:10.1016/S0377-0273(03)00232-4.

James, M. R., S. J. Lane, and S. B. Corder (2008) Modelling the rapid near-surface expansion of gas slugs in low-viscosity magmas, in *Fluid Motions in Volcanic Conduits: A Source of Seismic and Acoustic Signals*, edited by S. J. Lane and J. S. Gilbert, *Geol. Soc. Spec. Publ.*, *307*, 147–167.

James, M. R., S. J. Lane, L. Wilson, and S. B. Corder (2009), Degassing at low magma-viscosity volcanoes: Quantifying the transition between passive bubble-burst and Strombolian eruption, *J. Volcanol. Geotherm. Res.*, *180*, 81–88, doi:10.1016/j.jvolgeores.2008.09.002.

James, M. R., E. W. Llewellin, and S. J. Lane (2011), Comment on "It takes three to tango: 2. Bubble dynamics in basaltic volcanoes and ramification for modelling normal Strombolian activity" by J. Suckale et al., *J. Geophys. Res.*, *113*, B06207, doi:10.1029/2010JB008167.

Jaupart, C., and C. J. Allègre (1991), Gas content, eruption rate and instabilities of eruption regime in silici volcanoes, *Earth Planet. Sci. Lett.*, *102*, 413–429, doi:10.1016/0012-821X(91)90032-D.

Jaupart, C., and S. Vergniolle (1989), The generation and collapse of a foam layer at the roof of a basaltic magma chamber, *J. Fluid Mech.*, *203*, 347–380, doi:10.1017/S0022112089001497.

Kazahaya, K., H. Shinohara, K. Uto, M. Odai, Y. Makahori, H. Mori, H. Iino, M. Miyashita, and J. Hirabayashi (2004), Gigantic SO_2 emission from Miyakejima volcano, Japan, caused by caldera collapse, *Geology*, *32*, 425–428, doi:10.1130/G20399.1.

Keating, G., and G. Valentine (2008), Shallow plumbing systems for small-volume basaltic volcanoes, *Bull. Volcanol.*, *70*, 563–582, doi:10.1007/s00445-007-0154-1.

Kozma, R. (1995), Studies on the relationships between the statistics of void fraction fluctuations and the parameters of two-phase flows, *Int. J. Multiphase Flow*, *21*(2), 241–251, doi:10.1016/0301-9322(94)00077-W.

Lautze, N. C., and B. F. Houghton (2005), Physical mingling of magma and complex eruption dynamics in the shallow conduit at Stromboli volcano, Italy, *Geology*, *33*, 425–428, doi:10.1130/G21325.1.

Lehr, F., M. Millies, and D. Mewes (2002), Bubble-size distribution and flow fields in bubble columns, *AIChE J.*, *48*, 2426–2443, doi:10.1002/aic.690481103.

Liu, T. J. (1993), Bubble size and entrance length effects on void development in a vertical channel, *Int. J. Multiphase Flow*, *19*, 99–113, doi:10.1016/0301-9322(93)90026-Q.

Lucas, D., E. Krepper, and H.-M. Prasser (2005), Development of co-current air-water flow in a vertical pipe, *Int. J. Multiphase Flow*, *31*, 1304–1328, doi:10.1016/j.ijmultiphaseflow.2005.07.004.

Lyons, J. J., G. P. Waite, W. I. Rose, and G. Chigna (2010), Patterns in open vent, strombolian behavior at Fuego volcano, Guatemala, 2005–2007, *Bull. Volcanol.*, *72*, 1–15, doi:10.1007/s00445-009-0305-7.

Manga, M. (1996), Waves of bubbles in basaltic magmas and lavas, *J. Geophys. Res.*, *101*, 17,457–17,465, doi:10.1029/96JB01504.

Manga, M., and H. A. Stone (1994), Interaction between bubbles in magmas and lavas: Effects of bubble deformation, *J. Volcanol. Geotherm. Res.*, *63*, 267–279, doi:10.1016/0377-0273(94)90079-5.

Mangan, M. T., and K. V. Cashman (1996), The structure of basaltic scoria and reticulite and inferences for vesiculation, foam formation, and fragmentation in lava fountains, *J. Volcanol. Geotherm. Res.*, *73*, 1–18, doi:10.1016/0377-0273(96)00018-2.

McGonigle, A. J. S., C. Oppenheimer, A. R. Hayes, B. Galle, M. Edmonds, T. Caltabiano, G. Salerno, M. Burton, and T. A. Mather (2003), Sulphur dioxide fluxes from Mount Etna, Vulcano, and Stromboli measured with an automated scanning ultraviolet spectrometer, *J. Geophys. Res.*, *108*(B9), 2455, doi:10.1029/2002JB002261.

McQuillan, K. W., and B. Whalley (1985), Flow patterns in vertical two-phase flow, *Int. J. Multiphase Flow*, *11*, 161–175, doi:10.1016/0301-9322(85)90043-6.

Melnik, O., A. A. Barmin, and R. S. J. Sparks (2005), Dynamics of magma flow inside volcanic conduits with bubble overpressure buildup and gas loss through permeable magma, *J. Volcanol. Geotherm. Res.*, *143*, 53–68.

Menand, T., and J. C. Phillips (2007), Gas segregation in dikes and sills, *J. Volcanol. Geotherm. Res.*, *159*, 393–408, doi:10.1016/j.jvolgeores.2006.08.003.

Mishima, K., and M. Ishii (1984), Flow regime transition criteria for upward two-phase flow in vertical tubes, *Int. J. Heat Mass Transfer*, *27*(5), 723–737, doi:10.1016/0017-9310(84)90142-X.

Moody, L. F. (1944), Friction factors for pipe flow, *Trans. ASME*, *66*, 671–684.

Mudde, R. F., and T. Saito (2001), Hydrodynamical similarities between bubble column and bubbly type flow, *J. Fluid Mech.*, *437*, 203–228, doi:10.1017/S0022112001004335.

Muller, F. L., and J. F. Davidson (1992), On the contribution of small bubbles to mass transfer in bubble columns containing highly viscous liquids, *Chem. Eng. Sci.*, *47*(13–14), 3525–3532, doi:10.1016/0009-2509(92)85066-K.

Nishikawa, M. (1991), On the estimation of average shear rate in bubble columns, *Biotechnol. Bioeng.*, *37*, 691–692, doi:10.1002/bit.260370711.

Nusselt, W. A. (1916), The surface condensation of water vapor, *Z. Ver. Deutsch. Ing.*, *60*, 541–546.

Ohnesorge, W. (1936), Formation of drops by nozzles and the breakup of liquid jets, *Z. Angew. Math. Mech.*, *16*, 355–358, doi:10.1002/zamm.19360160611.

Ohnuki, A., and H. Akimoto (2000), Experimental study on transition of flow pattern and phase distribution in upward air-water two-phase flow along a large vertical pipe, *Int. J. Multiphase Flow*, *26*, 367–386, doi:10.1016/S0301-9322(99)00024-5.

Olmos, E., C. Gentric, C. Vial, G. Wild, and N. Midoux (2001), Numerical simulation of multiphase flow in bubble column reactors. Influence of bubble coalescence and break-up, *Chem. Eng. Sci.*, *56*, 6359–6365, doi:10.1016/S0009-2509(01)00204-4.

Omebere-Iyari, N. K., B. J. Azzopardi, and Y. Ladam (2007), Two-phase flow patterns in large diameter vertical pipes at high pressures, *AIChE J.*, *53*, 2493–2504, doi:10.1002/aic.11288.

Paglianti, A., M. Giona, and A. Soldati (1996), Characterization of subregimes in two-phase slug flow, *Int. J. Multiphase Flow*, *22*(4), 783–796, doi:10.1016/0301-9322(96)00019-5.

Pandit, A. B., J. Philip, J. F. Davidson, and P. W. Dodd (1987), The generation of small bubbles in liquids, *Rec. Trends Chem. Reaction Eng.*, *2*, 72–82.

Parfitt, E. A. (2004), A discussion on the mechanisms of explosive basaltic eruptions, *J. Volcanol. Geotherm. Res.*, *134*, 77–107, doi:10.1016/j.jvolgeores.2004.01.002.

Parfitt, E. A., and L. Wilson (1995), Explosive volcanic eruptions IX- the transition between Hawaiian-style lava fountaining and strombolian explosive activity, *Geophys. J. Int.*, *121*, 226–232, doi:10.1111/j.1365-246X.1995.tb03523.x.

Pioli, L., B. J. Azzopardi, and K. V. Cashman (2009), Controls on the explosivity of scoria cone eruptions: Magma segregation at conduit junctions, *J. Volcanol. Geotherm. Res.*, *186*, 407–415, doi:10.1016/j.jvolgeores.2009.07.014.

Polacci, M., R. A. Corsaro, and D. Andronico (2006), Coupled textural and compositional characterization of basaltic scoria: Insights into the transition from Strombolian to fire fountain activity at Mount Etna, Italy, *Geology*, *34*, 201–204, doi:10.1130/G22318.1.

Prince, M. J., and H. W. Blanch (1990), Bubble coalescence and break-up in air-sparged columns, *AIChE J.*, *36*, 1485–1499, doi:10.1002/aic.690361004.

Ripepe, M., A. J. L. Harris, and R. Carniel (2002), Thermal, seismic and infrasonic evidences of variable degassing rates at Stromboli volcano, *J. Volcanol. Geotherm. Res.*, *118*, 285–297, doi:10.1016/S0377-0273(02)00298-6.

Ripepe, M., D. Delle Donne, A. Harris, and E. Marchetti (2008), Dynamics of Strombolian activity, in *The Stromboli Volcano: An Integrate Study of the 2002–2003 Eruption*, *Geophys. Monogr. Ser.*, vol. 182, edited by S. Calvari et al., pp. 39–48, AGU, Washington D. C.

Ripepe, M., E. Marchetti, C. Bonadonna, A. J. L. Harris, L. Pioli, and G. Ulivieri (2010), Monochromatic infrasonic tremor driven by persistent degassing and convection at Villarrica Volcano, Chile, *Geophys. Res. Lett.*, *37*, L15303, doi:10.1029/2010GL043516.

Rust, A. C., and K. V. Cashman (2004), Permeability of vesicular silicic magma: Inertial and hysteresis effects, *Earth Planet. Sci. Lett.*, *228*, 93–107, doi:10.1016/j.epsl.2004.09.025.

Ruzicka, M. C., J. Zahradník, J. Drahos, and N. H. Thomas (2001), Homogeneous-heterogeneous regime transition in bubble columns, *Chem. Eng. Sci.*, *56*, 4609–4626, doi:10.1016/S0009-2509(01)00116-6.

Ryan, M. P. (1988), The mechanics and three-dimensional internal structure of active magmatic systems: Kilauea volcano, Hawaii, *J. Geophys. Res.*, *93*, 4213–4248, doi:10.1029/JB093iB05p04213.

Saar, M. O., and M. Manga (1999), Permeability-porosity relationships in vesiculating basalts, *Geophys. Res. Lett.*, *26*, 111–114, doi:10.1029/1998GL900256.

Sawyer, G. M., S. A. Carn, V. I. Tsanev, and C. Oppenheimer (2008), Investigation into magma degassing as Nyiragongo volcano, Democratic republic of the Congo, *Geochem. Geophys. Geosyst.*, *9*, Q02017, doi:10.1029/2007GC001829.

Seyfried, R., and A. Freundt (2000), Experiments on conduit flow and eruption behavior of basaltic volcanoes, *J. Geophys. Res.*, *105*, 23,727–23,740, doi:10.1029/2000JB900096.

Shen, X., R. Matsui, K. Mishima, and H. Nakamura (2010), Distribution parameter and drift velocity for two-phase flow in a large diameter pipe, *Nucl. Eng. Des.*, *240*, 3991–4000, doi:10.1016/j.nucengdes.2010.01.004.

Song, C. H., H. C. No, and M. K. Chung (1995), Investigation of bubble flow developments and its transitions based on the instability of void fraction waves, *Int. J. Multiphase Flow*, *21*(3), 381–404, doi:10.1016/0301-9322(94)00079-Y.

Sparks, R. J. S. (1978), The dynamics of bubble formation and growth in magmas: A review and analysis, *J. Volcanol. Geotherm. Res.*, *3*, 1–37, doi:10.1016/0377-0273(78)90002-1.

Spedding, P. L., G. S. Woods, R. S. Raghunathan, and J. K. Watterson, (1998), Vertical two-phase flow. Part I: Flow regimes, *Trans. Inst. Chem. Eng.*, *76*(A), 612–619.

Stein, D. J., and F. J. Spera (1992), Rheology and microstructure of magmatic emulsions: Theory and experiments, *J. Volcanol. Geotherm. Res.*, *49*, 157–174, doi:10.1016/0377-0273(92)90011-2.

Stevenson, D. S., and S. Blake (1998), Modelling the dynamics and thermodynamics of volcanic degassing, *Bull. Volcanol.*, *60*, 307–317, doi:10.1007/s004450050234.

Taitel, Y., D. Barnea, and A. E. Dukler (1980), Modelling flow pattern transition for steady upward gas-liquid flow in vertical tubes, *AIChE J.*, *26*, 345–354, doi:10.1002/aic.690260304.

Van den Hengel, E. I. V., N. G. Deen, and J. A. M. Kuipers (2005), Application of coalescence and breakup models in a discrete bubble model for bubble columns, *Ind. Eng. Chem. Res.*, *44*, 5233–5245, doi:10.1021/ie0492449.

Vergniolle, S., and G. Brandeis (1996), Strombolian explosions 1. A large bubble breaking at the surface of a lava column as a source of sound, *J. Geophys. Res.*, *101*, 20,433–20,447, doi:10.1029/96JB01178.

Vergniolle, S., and C. Jaupart (1986), Separated two-phase flow and basaltic eruptions, *J. Geophys. Res.*, *91*, 12,842–12,860, doi:10.1029/JB091iB12p12842.

Vergniolle, S., and M. Mangan (2000), Hawaiian and Strombolian eruptions, in *Encyclopedia of Volcanoes*, edited by B. Houghton et al., pp. 447–461, Academic, San Diego, Calif.

Viana, F., R. Pardo, R. Zaney, J. L. Trallero, and D. D. Joseph (2003), Universal correlation for the rise velocity of long gas bubbles in round pipes, *J. Fluid Mech.*, *494*, 379–398, doi:10.1017/S0022112003006165.

Vijayan, M., S. Jayanti, and A. R. Balakrishnan (2001), Effect of tube diameter on flooding, *Int. J. Multiphase Flow*, *27*, 797–816, doi:10.1016/S0301-9322(00)00045-8.

Wallis, G. B. (1969), *One-Dimensional Two-Phase Flow*, 410 pp., McGraw-Hill, New York.

Whalley, P. B. (1986), *Boiling, Condensation, and Gas-liquid Flow*, 291 pp., Clarendon, Oxford, U. K.

White, E. T., and R. H. Beardmore (1962), The velocity of rise of single cylindrical air bubbles through liquids contained in vertical tubes, *Chem. Eng. Sci.*, *17*, 351–361, doi:10.1016/0009-2509(62)80036-0.

Wilson, L., and J. W. Head III (1981), Ascent and eruption of basaltic magma on the Earth and Moon, *J. Geophys. Res.*, *86*, 2971–3001.

Woldesemayat, M. A., and A. J. Ghajar (2007), Comparison of void fraction correlations for different flow patterns in horizontal and upward inclined pipes, *Int. J. Multiphase Flow*, *33*, 347–370, doi:10.1016/j.ijmultiphaseflow.2006.09.004.

Zapke, A., and D. G. Kröger (1996), The influence of fluid properties and inlet geometry on flooding in vertical and inclined tubes, *Int. J. Multiphase Flow*, *22*(3), 461–472, doi:10.1016/0301-9322(95)00076-3.

Zapke, A., and D. G. Kröger (2000), Countercurrent gas–liquid flow in inclined and vertical ducts - II: The validity of the Froude-Ohnesorge number correlation for flooding, *Int. J. Multiphase Flow*, *26*, 1457–1468, doi:10.1016/S0301-9322(99)00098-1.

Zuber, N., and J. A. Findlay (1965), Average volumetric concentration in two-phase flow systems, *J. Heat Transfer*, *87*, 453–468.

Zuber, N., and J. Hench (1962), Steady state and transient void fraction of bubbling systems and their operating limit. Part 1: Steady state operation, *Rep. 62GL100*, Gen. Electr., Washington, D. C.

B. J. Azzopardi, Process and Environmental Engineering Research Division, Faculty of Engineering, University of Nottingham, University Park, Nottingham NG7 2RD, UK.

C. Bonadonna and L. Pioli, Section des Sciences de la Terre et de l'Environnement, Université de Genève, Rue des Maraîchers 13, CH-1205 Genève, Switzerland. (Laura.Pioli@unige.ch)

J. C. Phillips, Department of Earth Sciences, University of Bristol, Wills Memorial Building, Queen's Road, Bristol BS8 1RJ, UK.

M. Ripepe, Dipartimento di Scienze della Terra, Università di Firenze, v. La Pira 4, I-50121 Florence, Italy.